B physics

Valerie Gibson

University of Cambridge, U.K.

1 Introduction

Since the discovery of the b quark, its properties and interactions have been studied in great detail. One major observation is that the b quark has a very long lifetime, $\mathcal{O}(10^{-12})$ ps, thereby implying a hierarchy in the mixing between quark generations. This, together with the discovery of CP violation, has led to the main goal of the current generation of B physics practitioners; namely to understand the structure of quark mixing and its rôle in CP violation.

The physical importance of CP violation is demonstrated by the fact that it is one of the necessary ingredients to explain the dominance of matter over antimatter in our universe (Sakharov 1967). Although the Standard Model naturally accommodates CP violation through the complex quark mixing matrix (Kobayashi and Maskawa 1972), it alone can not explain the large asymmetry observed (Shaposhnikov 1986). However, baryogenesis at the electro-weak scale is still possible with various extensions to the Standard Model which introduce additional sources of CP violation (Nir 1999).

Experimentally, CP violation was unexpectedly discovered in the decay of neutral kaons in 1964 (Christenson 1964). Since then, the kaon system remained the only place CP violation had been observed until 2001 when it was observed in the b quark system for the first time by the B factory experiments, BaBar (BaBar 2001) and Belle (Belle 2001). In the B meson system, CP violation is expected to occur in many different decay channels and for some the Standard Model can make precise predictions. Therefore, the B system is considered an ideal place to test the Standard Model predictions and to hunt for the necessary new physics beyond.

These lectures focus on how B decays can be used to obtain a better understanding of the Standard Model description of quark mixing and CP violation, to search for new physics beyond the Standard Model and to provide a strategy to disentangle cleanly the new physics and the Standard Model contributions.

2 Mixing and CP Violation

We start with a gentle introduction to the phenomenology of neutral meson mixing and CP violation. There are many excellent review articles on this topic; see for example (BaBar 1998 and Nir 2001). Here we describe a general approach that is applicable to any neutral meson system.

2.1 Neutral Meson Mixing

The phenomenon of oscillations between neutral meson particle and antiparticle is well established and is possible as a result of the non-conservation of flavour in the weak interaction. Consider the time development of an arbitrary neutral meson state, X^0, and its antiparticle, $\overline{X^0}$,

$$a(t)\ |X^0\rangle + b(t)\ |\overline{X^0}\rangle, \tag{1}$$

which is governed by the time-dependent differential equation

$$i\frac{\partial}{\partial t}\begin{pmatrix} a \\ b \end{pmatrix} = H\begin{pmatrix} a \\ b \end{pmatrix} = \begin{pmatrix} M_{11} - \frac{i}{2}\Gamma_{11} & M_{12} - \frac{i}{2}\Gamma_{12} \\ M_{12}^* - \frac{i}{2}\Gamma_{12}^* & M_{22} - \frac{i}{2}\Gamma_{22} \end{pmatrix}\begin{pmatrix} a \\ b \end{pmatrix}. \tag{2}$$

Here M_{ij} and Γ_{ij} are elements of the so-called mass and decay matrices respectively and are associated with measurable quantities. A consequence of the invariance of the combined symmetry operation CPT is that particle and antiparticle masses and lifetimes are identical, namely $M_{11} = M_{22} \equiv M$ and $\Gamma_{11} = \Gamma_{22} \equiv \Gamma$.

The eigenstates of H, $|X_1\rangle$ and $|X_2\rangle$, can be written as a linear combination of the particle and antiparticle states,

$$\begin{aligned} |X_1\rangle &= p\ |X^0\rangle + q\ |\overline{X^0}\rangle \\ |X_2\rangle &= p\ |X^0\rangle - q\ |\overline{X^0}\rangle, \end{aligned} \tag{3}$$

where p and q represent the amount of meson state mixing and are complex numbers with the normalization condition $|p|^2 + |q|^2 = 1$. The eigenvalues of $|X_{1,2}\rangle$, $E_{1,2}$, are then obtained from the characteristic equation,

$$|H - EI| = 0, \tag{4}$$

where I is a 2×2 unit matrix. The eigenvalues obtained are

$$\begin{aligned} E_{1,2} &= M_{1,2} - \frac{i}{2}\Gamma_{1,2} = M - \frac{i}{2}\Gamma \pm \sqrt{(M_{12} - \frac{i}{2}\Gamma_{12})(M_{12}^* - \frac{i}{2}\Gamma_{12}^*)} \\ &= \left(M \mp \frac{\Delta M}{2}\right) - \frac{i}{2}\left(\Gamma \mp \frac{\Delta\Gamma}{2}\right) \end{aligned} \tag{5}$$

where $M_{1,2}$ and $\Gamma_{1,2}$ are the masses and decay widths of the two eigenstates and $\Delta M = M_2 - M_1$ and $\Delta\Gamma = \Gamma_2 - \Gamma_1$. The relationship between p and q can be extracted from the eigenvector equations,

$$(H - EI)\begin{pmatrix} p \\ \pm q \end{pmatrix} = 0, \tag{6}$$

where

$$\frac{q}{p} = \sqrt{\frac{M_{12}^* - \frac{i}{2}\Gamma_{12}^*}{M_{12} - \frac{i}{2}\Gamma_{12}}}. \tag{7}$$

The time evolution of the initial particle and antiparticle states, $|X^0(t)\rangle$ and $|\overline{X^0}(t)\rangle$, obtained by rearranging equations (3), and substituting for the time evolution of the states $|X_{1,2}\rangle$,

$$|X_{1,2}(t)\rangle = |X_{1,2}\rangle\, e^{-i(M_{1,2}-\frac{i}{2}\Gamma_{1,2})t}, \tag{8}$$

are

$$\begin{aligned} |X^0(t)\rangle &= f_+(t)\,|X^0\rangle + \frac{q}{p}f_-(t)\,|\overline{X^0}\rangle \\ |\overline{X^0}(t)\rangle &= f_+(t)\,|\overline{X^0}\rangle + \frac{p}{q}f_-(t)\,|X^0\rangle, \end{aligned} \tag{9}$$

where $f_\pm(t) = \frac{1}{2}\left[e^{-i(M_1-\frac{i}{2}\Gamma_1)t} \pm e^{-i(M_2-\frac{i}{2}\Gamma_2)t}\right]$. Hence, the probabilities of finding an $|X^0\rangle$ and an $|\overline{X^0}\rangle$ at time t from an initially pure $|X^0\rangle$ state are

$$\begin{aligned} P(X^0 \to X^0 : t) &= |\langle X^0|X^0(t)\rangle|^2 = |f_+(t)|^2 \\ P(X^0 \to \overline{X^0} : t) &= |\langle \overline{X^0}|X^0(t)\rangle|^2 = |\frac{q}{p}f_-(t)|^2 \end{aligned} \tag{10}$$

with

$$|f_\pm(t)|^2 = \frac{1}{4}\left[e^{-\Gamma_1 t} + e^{-\Gamma_2 t} \pm 2e^{-\overline{\Gamma}t}\cos(\Delta M t)\right] \tag{11}$$

and the average decay width $\overline{\Gamma} = (\Gamma_1+\Gamma_2)/2$. The last term in equation (11) describes the oscillation character of the X^0 and $\overline{X^0}$ content in an initial pure X^0 beam. The oscillations depend crucially on the size of the oscillation parameter, defined as $x = |\Delta M|/\overline{\Gamma}$. Shown in Figure 1 are the probabilities (assuming $|q/p| = 1$) for finding an X^0 and an $\overline{X^0}$ from an initial X^0 state as a function of time. When $x = 1$, there is some probability that the meson will oscillate before it decays, and when $x = 25$, the meson exhibits very rapid oscillations before decaying. Figure 1a) corresponds approximately to $K^0 - \overline{K^0}$ mixing, in which the difference in lifetimes and hence decay widths of the two physical eigenstates (K_S^0 and K_L^0) is large due to the domination of $K_S^0 \to \pi\pi$ final states,

$$\frac{\tau_L}{\tau_S} = \frac{51.7 \pm 0.4 \text{ ns}}{0.08927 \pm 0.00009 \text{ ns}} \sim 580, \tag{12}$$

and the mass difference,

$$\Delta M = M_L - M_S = (3.483 \pm 0.009) \times 10^{-15} \text{ GeV}, \tag{13}$$

is very small (Particle Data Group 2002). Figure 1b) and 1c) correspond approximately to $B_d^0 - \overline{B_d^0}$ and $B_s^0 - \overline{B_s^0}$ meson mixing respectively. In contrast to the kaon system, the overwhelming majority of final states expected for B^0 decays are the same as for the $\overline{B^0}$ decays and hence the lifetimes of the physical eigenstates are expected to be approximately the same (Particle Data Group 2002),

$$\left(\frac{\Delta\Gamma}{\overline{\Gamma}}\right)_{\rm d} \sim 0.5\%, \quad \text{and} \quad \left(\frac{\Delta\Gamma}{\overline{\Gamma}}\right)_{\rm s} \sim 15\%. \tag{14}$$

However, the difference between the masses is large (HFAG 2003),

$$\Delta M_d = (3.30 \pm 0.04) \times 10^{-13}\ \text{GeV} \quad \text{and} \quad \Delta M_s > 9.5 \times 10^{-12}\ \text{GeV}\ (95\%\ cl), \tag{15}$$

and when combined with the measured B_d^0 and B_s^0 lifetimes, $\tau_d = (1.542 \pm 0.016)$ ps and $\tau_s = (1.461 \pm 0.057)$ ps (Particle Data Group 2002), result in oscillation parameters of $x_d = 0.77 \pm 0.02$ and $x_s > 21$ respectively.

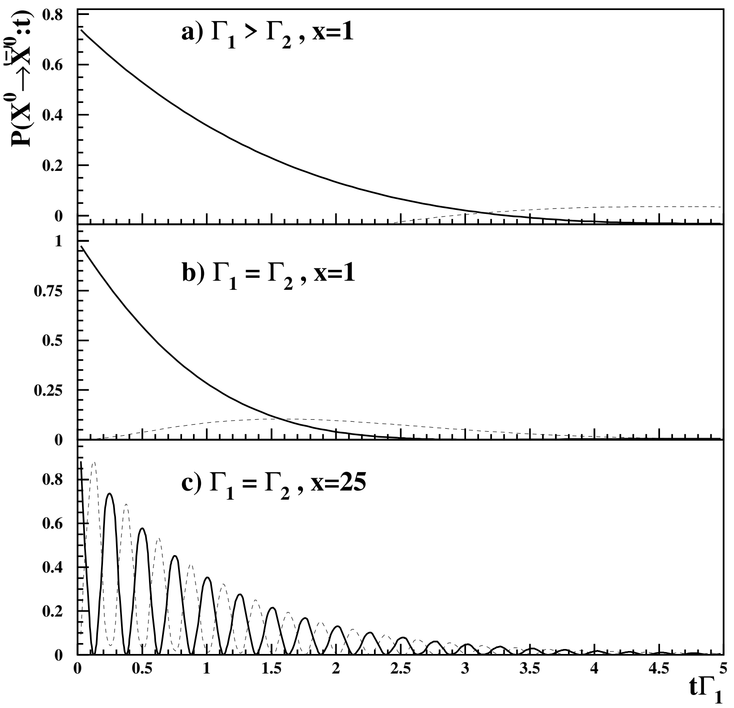

Figure 1. *The probability of finding an X^0 meson (solid curve) and an $\overline{X^0}$ meson (dashed curve) as a function of $t\Gamma_1$ from an initial pure X^0 state for the cases a) $\Gamma_1 > \Gamma_2$ with $x = 1$, b) $\Gamma_1 = \Gamma_2$ with $x = 1$ and c) $\Gamma_1 = \Gamma_2$ with $x = 25$.*

2.2 CP Violation in Meson Decays

We now consider the time dependent decay rates for the neutral mesons X^0 and $\overline{X^0}$ to decay into the same final state f,

$$\begin{aligned} \Gamma_f(t) &\equiv \Gamma\left(X^0(t) \to f\right) \\ &= |A_f|^2 \left[|f_+(t)|^2 + \left(\frac{q}{p}\frac{\overline{A_f}}{A_f}\right)^2 |f_-(t)|^2 + 2\mathrm{Re}\left\{\frac{q}{p}\frac{\overline{A_f}}{A_f} f_+^*(t) f_-(t)\right\}\right] \end{aligned} \tag{16}$$

and

$$\begin{aligned} \overline{\Gamma_f}(t) &\equiv \Gamma\left(\overline{X^0}(t) \to f\right) \\ &= |A_f|^2 \left[\left|\frac{\overline{A_f}}{A_f}\right|^2 |f_+(t)|^2 + \left(\frac{p}{q}\right)^2 |f_-(t)|^2 + 2\left(\frac{p}{q}\right)^2 \mathrm{Re}\left\{\frac{q}{p}\frac{\overline{A_f}}{A_f}^* f_+^*(t) f_-(t)\right\}\right], \end{aligned} \tag{17}$$

where, $A_f = \langle f|H|X^0\rangle$ and $\overline{A_f} = \langle f|H|\overline{X^0}\rangle$ are the instantaneous decay amplitudes. Any difference between these two rates is clear proof of CP violation.

The first terms in the rates Γ_f and $\overline{\Gamma_f}$ show that CP violation is generated if $|A_f| \neq |\overline{A_f}|$. This is called *CP violation in the decay amplitudes.* The second terms of Γ_f and $\overline{\Gamma_f}$ show that CP violation is generated if $|q/p| \neq 1$, even if there is no CP violation in the decay amplitudes. From equations (10), it is clear that if $|q/p| \neq 1$, then the oscillation rate for $X^0 \to \overline{X^0}$ is different from that for $\overline{X^0} \to X^0$. This type of CP violation is called *CP violation in the mixing* and results in two physical eigenstates which are different from the CP eigenstates. Finally, if there is no CP violation in the mixing or decay amplitudes, the first and second terms of Γ_f and $\overline{\Gamma_f}$ are identical. However, CP violation can still arise due to the third term which can be expanded using

$$\mathrm{Re}\left\{\left(\frac{q}{p}\frac{\overline{A_f}}{A_f}\right)^{(*)} f_+^*(t)f_-(t)\right\} = \mathrm{Re}\left\{\frac{q}{p}\frac{\overline{A_f}}{A_f}\right\}\mathrm{Re}\left\{f_+^*(t)f_-(t)\right\} \mp \mathrm{Im}\left\{\frac{q}{p}\frac{\overline{A_f}}{A_f}\right\}\mathrm{Im}\left\{f_+^*(t)f_-(t)\right\}. \tag{18}$$

In this case, if

$$\mathrm{Im}\left\{\frac{q}{p}\frac{\overline{A_f}}{A_f}\right\} \neq 0, \tag{19}$$

then Γ_f and $\overline{\Gamma_f}$ differ resulting in CP violation. Since the process involves the decays of $X^0(\overline{X^0})$ from the initial $X^0(\overline{X^0})$ and the decays of the $\overline{X^0}(X^0)$ oscillated from the initial $X^0(\overline{X^0})$ into a common final state, this type of CP violation is commonly referred to as *CP violation in the interference between the mixing and decay amplitudes.*

Complementary to this classification of CP violation is the widely used notation of *direct* versus *indirect* CP violation. It was motivated historically by the hypothesis of a new superweak interaction that was supposed to account for CP violation in $K_L^0 \to \pi^+\pi^-$ decays (Wolfenstein 1964). *Indirect* CP violation is any CP violating effect that can be entirely attributed to CP violation in the neutral meson mass matrix and is independent of the final state. Conversely, any effect that can not be described in this way and explicitly requires CP violating phases in the decay amplitude itself and hence depends on the final state is called *direct CP violation.* It follows that CP violation in the mixing represents indirect CP violation, CP violation in the decay is direct CP violation and CP violation in the interference contains aspects of both indirect and direct CP violation.

In the B system, where $\Delta\Gamma$ is small, it is convenient to derive the time dependent decay rates from the particle-antiparticle base,

$$\Gamma_f(t) = \frac{|A_f|^2}{2} e^{-\overline{\Gamma}t}\left[I_+(t) + I_-(t)\right] \tag{20}$$

and

$$\overline{\Gamma_f}(t) = \frac{|\overline{A_f}|^2}{2|\lambda|^2} e^{-\overline{\Gamma}t}\left[I_+(t) - I_-(t)\right], \tag{21}$$

where the two time dependent functions $I_\pm(t)$ are given by

$$I_+(t) = \left(1+|\lambda|^2\right)\cosh\left(\frac{\Delta\Gamma t}{2}\right) + 2\mathrm{Re}\left\{\lambda\right\}\sinh\left(\frac{\Delta\Gamma t}{2}\right) \tag{22}$$

$$I_-(t) = \left(1-|\lambda|^2\right)\cos\left(\Delta M t\right) + 2\mathrm{Im}\left\{\lambda\right\}\sin\left(\Delta M t\right). \tag{23}$$

The complex quantity λ,

$$\lambda = \frac{q}{p}\frac{\overline{A_f}}{A_f}, \tag{24}$$

has observable real and imaginary parts that quantify CP violation. Similarly, the corresponding decay amplitudes for the CP conjugated final states $\bar{f}$ are given by

$$\Gamma_{\bar{f}}(t) = \frac{|A_{\bar{f}}|^2}{2|\overline{\lambda}|^2} e^{-\overline{\Gamma}t}\left[\overline{I}_+(t) - \overline{I}_-(t)\right] \tag{25}$$

and

$$\overline{\Gamma_{\bar{f}}}(t) = \frac{|\overline{A_{\bar{f}}}|^2}{2} e^{-\overline{\Gamma}t}\left[\overline{I}_+(t) + \overline{I}_-(t)\right], \tag{26}$$

where $\overline{I}_{\pm}(t)$ are the same as $I_{\pm}(t)$ but with λ replaced by

$$\overline{\lambda} = \frac{p}{q}\frac{A_{\bar{f}}}{\overline{A_{\bar{f}}}}. \tag{27}$$

We will now consider the three categories of CP violation in turn.

2.2.1 CP Violation in the Mixing

The test of CP invariance through meson state mixing is whether the magnitudes of the off-diagonal elements of the mass and decay matrices are the same, namely,

$$|M_{12} - \frac{i}{2}\Gamma_{12}| \stackrel{?}{=} |M_{12}^* - \frac{i}{2}\Gamma_{12}^*|. \tag{28}$$

If they are not the same, it physically corresponds to a difference in the mixing rates between $X^0 \to \overline{X^0}$ and $\overline{X^0} \to X^0$. Equation (7) implies that if

$$\left|\frac{q}{p}\right| \neq 1 \tag{29}$$

then CP is violated in the meson state mixing. A difference in the mixing rates will occur when there is a phase difference between M_{12} and Γ_{12}. The standard convention is to keep Γ_{12} real and describe any observed CP violation by a small imaginary part of M_{12}.

CP violation in the mixing has been measured in the K^0 semi-leptonic charge decay asymmetry (Particle Data Group 2002),

$$\mathcal{A}_{sl} = \frac{\Gamma\left(K_L^0 \to \pi^-\ell^+\nu\right) - \Gamma\left(K_L^0 \to \pi^+\ell^-\nu\right)}{\Gamma\left(K_L^0 \to \pi^-\ell^+\nu\right) + \Gamma\left(K_L^0 \to \pi^+\ell^-\nu\right)} = 0.327 \pm 0.012\% = \frac{1 - |q/p|^2}{1 + |q/p|^2}. \tag{30}$$

We can interpret this result in terms of the phase difference between M_{12} and Γ_{12}, if we define the phase ϕ_{12} according to

$$\frac{M_{12}}{\Gamma_{12}} = -\left|\frac{M_{12}}{\Gamma_{12}}\right| e^{i\phi_{12}} \tag{31}$$

and knowing that the CP violating effects in the K system are small ($\phi_{12} << 1$). We find that $\phi_{12} \approx 6.5 \times 10^{-3}$.

In principle, the semi-leptonic decay asymmetry can also be measured using B^0 decays,

$$\mathcal{A}_{sl} = \frac{\Gamma\left(\overline{B^0} \to \ell^- \nu X\right) - \Gamma\left(B^0 \to \ell^+ \nu X\right)}{\Gamma\left(\overline{B^0} \to \ell^- \nu X\right) + \Gamma\left(B^0 \to \ell^+ \nu X\right)} = \frac{1 - |q/p|^4}{1 + |q/p|^4}. \tag{32}$$

However, CP violation in the mixing is expected to be small in the B system due to GIM suppression and the smallness of $\Delta\Gamma$, $\mathcal{O}\left(10^{-3}\right)$ for B_d^0 and $\mathcal{O}\left(10^{-5}\right)$ for B_s^0, and the theoretical interpretation is difficult due to large hadronic uncertainties in Γ_{12}.

2.2.2 CP Violation in the Decay

CP violation in the decay is due to an interference among decay amplitudes and results in a difference between the partial decay rate $\mathrm{X} \to f$ and the charge conjugate process $\overline{\mathrm{X}} \to \overline{f}$. The two decay amplitudes are written as

$$A \equiv \langle f \,| H |\, \mathrm{X} \rangle, \qquad \overline{A} \equiv \langle \overline{f} \,| H |\, \overline{\mathrm{X}} \rangle; \tag{33}$$

and if several amplitudes contribute to A and $\overline{A}$, then

$$A = \sum_i A_i e^{i\phi_i} e^{i\delta_i} \quad \text{and} \quad \overline{A} = \sum_i A_i e^{-i\phi_i} e^{i\delta_i}, \tag{34}$$

where A_i are real. Two types of phases appear in A and $\overline{A}$. ϕ_i are parameters that violate CP and appear in A and $\overline{A}$ with opposite signs. Usually they arise in the electroweak sector and hence are known as *weak phases.* δ_i are *strong phases* that arise in the scattering or decay amplitudes. They do not violate CP and appear in A and $\overline{A}$ with the same sign.

If a meson can decay by at least two different decay mechanisms with different amplitudes, having different weak and strong phases, there is an interference between the decay amplitudes resulting in

$$\left|\frac{\overline{A}}{A}\right| = \left|\frac{\sum_i A_i e^{-i\phi_i} e^{i\delta_i}}{\sum_i A_i e^{i\phi_i} e^{i\delta_i}}\right| \neq 1 \tag{35}$$

and corresponds to CP violation in the decay.

In principle, CP violation in the decay can be measured from the asymmetry in charged decays

$$\mathcal{A}_{+-} = \frac{\Gamma\left(X^+ \to f\right) - \Gamma\left(X^- \to \overline{f}\right)}{\Gamma\left(X^+ \to f\right) + \Gamma\left(X^- \to \overline{f}\right)} = \frac{1 - \left|\overline{A}/A\right|^2}{1 + \left|\overline{A}/A\right|^2}. \tag{36}$$

However, the theoretical prediction for $\mathcal{A}_{+-}$ is difficult due to hadronic uncertainties in the calculation of the strong phase difference. CP violation in the decay has, however, been observed through the measurement of $\mathrm{Re}\{\varepsilon'\}$ in $K^0 \to \pi^+\pi^-$ decays (see Section 2.2.4).

2.2.3 CP Violation in the Interference

CP violation in the interference between the mixing and decay amplitudes can be measured from the time dependent CP asymmetry,

$$\mathcal{A}(t) = \frac{\Gamma_f - \overline{\Gamma}_f}{\Gamma_f + \overline{\Gamma}_f} = \frac{I_-(t)}{I_+(t)} \tag{37}$$

$$= \frac{(1-|\lambda|^2)\cos(\Delta M t) + 2\mathrm{Im}\,\{\lambda\}\sin(\Delta M t)}{(1+|\lambda|^2)\cosh(\Delta\Gamma t/2) + 2\mathrm{Re}\,\{\lambda\}\sinh(\Delta\Gamma t/2)}. \tag{38}$$

This asymmetry can also be written so as to separate the direct CP violating contribution, $\mathcal{A}_{\rm CP}^{dir}$, from that describing CP violation in the interference between the mixing and decay amplitudes, $\mathcal{A}_{\rm CP}^{mix}$,

$$\mathcal{A}(t) = \mathcal{A}_{\rm CP}^{dir}\cos(\Delta M t) + \mathcal{A}_{\rm CP}^{mix}\sin(\Delta M t). \tag{39}$$

In the B system, where $\Delta\Gamma$ is small,

$$\mathcal{A}_{\rm CP}^{dir} = \frac{(1-|\lambda|^2)}{(1+|\lambda|^2)} \quad \text{and} \quad \mathcal{A}_{\rm CP}^{mix} = \frac{2\mathrm{Im}\,\{\lambda\}}{(1+|\lambda|^2)}. \tag{40}$$

Furthermore, for decays dominated by a single CP violating phase, $A_{\rm CP}^{dir}$ is negligible and the CP asymmetry reduces to

$$\mathcal{A}(t) = \mathrm{Im}\,\{\lambda\}\sin(\Delta M t). \tag{41}$$

In this case, $\mathrm{Im}\,\{\lambda\}$ is the phase difference between the mixing amplitude and the phase of the relevant decay amplitude and can be cleanly interpreted in terms of purely electroweak parameters.

CP violation in the interference has been observed in K^0 decays and has approximately the same magnitude, $\mathcal{O}(10^{-3})$, as CP violation in the mixing (Nakada 2002). Most recently, CP violation in the interference has been observed in the B system by the B factory experiments where a relatively large CP asymmetry has been measured (see Section 5.3).

2.2.4 The Parameters ε and ε'

The parameters ε and ε' are normally used to describe CP violation in K^0 decays (Nakada 2002) (Particle Data Group 2002). However, the underlying processes producing CP violation in the K^0 and B^0 system are the same. Therefore, it is a useful exercise to translate the language of ε and ε' into the λ notation we have used here.

In the K^0 system, the CP observables

$$\eta_{+-} \equiv \frac{A(K_L^0 \to \pi^+\pi^-)}{A(K_S^0 \to \pi^+\pi^-)} \quad \text{and} \quad \eta_{00} \equiv \frac{A(K_L^0 \to \pi^0\pi^0)}{A(K_S^0 \to \pi^0\pi^0)}, \tag{42}$$

are related to λ by

$$\eta_f = \frac{1-\lambda_f}{1+\lambda_f}, \tag{43}$$

and are therefore affected by all 3 types of CP violation. In principle, we could define similar parameters for the B system, such as,

$$\begin{aligned} \eta_{+-} &\equiv \frac{A(B_H \to \pi^+\pi^-)}{A(B_L \to \pi^+\pi^-)}, \quad \eta_{00} \equiv \frac{A(B_H \to \pi^0\pi^0)}{A(B_L \to \pi^0\pi^0)} \\ \text{and} \quad \eta_{J/\psi K_S^0} &\equiv \frac{A(B_H \to J/\psi K_S^0)}{A(B_L \to J/\psi K_S^0)} \quad etc \end{aligned} \tag{44}$$

where B_H and B_L are the B^0 mass eigenstates (see Section 3.1).

Instead of η_{+-} and η_{00}, the parameters ε and ε' are defined such that any direct CP violating effects are isolated into ε',

$$\varepsilon \equiv \frac{1}{3}(\eta_{00} + 2\eta_{+-}), \quad \varepsilon' \equiv \frac{1}{3}(\eta_{+-} - \eta_{00}). \tag{45}$$

In the two pion final state, two isospin terms ($I = 0, 2$) contribute to the decay amplitudes,

$$A_I = \langle(\pi\pi)_I|H|X^0\rangle \quad \text{and} \quad \overline{A_I} = \langle(\pi\pi)_I|H|\overline{X^0}\rangle. \tag{46}$$

Since the measured amplitude ratio $|A_2/A_0| << 1$, it follows that to first order in A_2/A_0,

$$\varepsilon \approx \frac{1-\lambda_0}{1+\lambda_0}, \tag{47}$$

where $\lambda_0 = \frac{q}{p}\frac{\overline{A_0}}{A_0}$. Therefore, since λ_0 depends only on a single final state, ε does not contain CP violation in the decay. We can show that

$$\mathrm{Re}\{\varepsilon\} \approx \frac{1}{2}\left[1 - \left|\frac{q}{p}\right|\right] \approx \frac{\phi_{12}}{4} \tag{48}$$

and

$$\mathrm{Im}\{\varepsilon\} \approx \frac{1}{2}\mathrm{Im}\left\{\frac{q}{p}\frac{\overline{A_0}}{A_0}\right\} \approx \frac{\phi_{12}}{4}. \tag{49}$$

Hence, $\mathrm{Re}\{\varepsilon\}$ and $\mathrm{Im}\{\varepsilon\}$ correspond to CP violation in the mixing and interference respectively with approximately the same order of magnitude, $\mathcal{O}(10^{-3})$.

From the definitions of ε and ε' it can be shown that

$$\eta_{+-} \approx \varepsilon + \varepsilon' \tag{50}$$

which leads to

$$\lambda_{+-} \approx 1 - 2\varepsilon - 2\varepsilon' \tag{51}$$

and

$$|\lambda_{+-}|^2 \approx 1 - 4\mathrm{Re}\{\varepsilon\} - 4\mathrm{Re}\{\varepsilon'\}. \tag{52}$$

Using equation (48), we find

$$\mathrm{Re}\{\varepsilon'\} = \frac{1}{4}\left[1 - \left|\frac{\overline{A_{+-}}}{A_{+-}}\right|^2\right] \tag{53}$$

and

$$\mathrm{Im}\,\{\varepsilon'\} = \left[\frac{1}{2}\mathrm{Im}\,\{\lambda_{+-}\} + \mathrm{Im}\,\{\varepsilon\}\right]. \tag{54}$$

Hence, $\mathrm{Re}\,\{\varepsilon'\}$ and $\mathrm{Im}\,\{\varepsilon'\}$ correspond to CP violation in the decay and CP violation in the interference respectively. The $\mathrm{Re}\,\{\varepsilon'\}$ has been measured in $K^0 \to \pi\pi$ decays and, after 37 years of precision experiments, has culminated in a world average (Particle Data Group 2003) of

$$\mathrm{Re}\,\{\varepsilon'\} = (16.7 \pm 2.3) \times 10^{-4} \tag{55}$$

which is clear proof that CP violation in the decay exists in the kaon system. In a similar way, we could define

$$\varepsilon'_B = \frac{1}{3}(\eta_{+-} - \eta_{00}) \;\text{ or }\; \varepsilon'_B = \frac{1}{3}(\eta_{+-} - \eta_{J/\psi K^0_S}) \tag{56}$$

for the B^0 system. Indeed, any measurement of a non-zero value of ε'_B would be evidence for direct CP violation.

3 Weak Decays in the Standard Model

In the Standard Model with three fermion families, the weak charged current can be written as

$$J_\mu = (\bar{u}, \bar{c}, \bar{t})_L\, \gamma_\mu\, V_{\mathrm{CKM}} \begin{pmatrix} d \\ s \\ b \end{pmatrix}_L \tag{57}$$

where V_{CKM} is the unitary $3{\times}3$ Cabibbo-Kobayashi-Maskawa (CKM) quark mixing matrix (Cabibbo 1963) (Kobayashi and Maskawa 1972) and describes the rotation between the weak eigenstates (d', s', b') and the mass eigenstates (d, s, b),

$$\begin{pmatrix} d' \\ s' \\ b' \end{pmatrix} = V_{\mathrm{CKM}} \begin{pmatrix} d \\ s \\ b \end{pmatrix}. \tag{58}$$

The CKM matrix can be written explicitly as

$$V_{\mathrm{CKM}} = \begin{pmatrix} V_{ud} & V_{us} & V_{ub} \\ V_{cd} & V_{cs} & V_{cb} \\ V_{td} & V_{ts} & V_{tb} \end{pmatrix} \tag{59}$$

where V_{ij} is the matrix element coupling the i^{th} up-type quark to the j^{th} down-type quark. The magnitudes of seven of the nine matrix elements, $|V_{ud}|$, $|V_{us}|$, $|V_{ub}|$, $|V_{cd}|$, $|V_{cs}|$, $|V_{cb}|$ and $|V_{tb}|$ are determined from nuclear β decay and pion, kaon, hyperon, D meson, B meson and top quark decays assuming first order (tree-level) weak interactions. The remaining two elements, $|V_{td}|$ and $|V_{ts}|$, can only be accessed through box diagrams or through second order weak interactions such as the QCD penguin diagrams which generate rare B hadron decay modes. Examples of Feynman diagrams for tree-level, box and penguin B decays are shown in Figure 2.

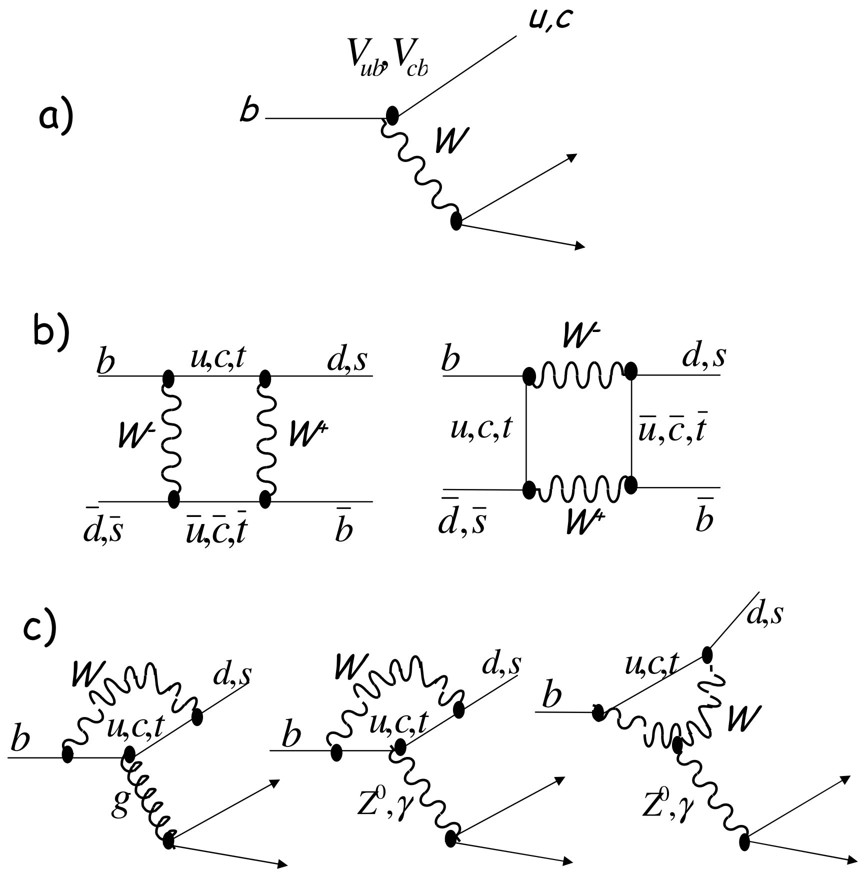

Figure 2. *The Standard Model B decay diagrams. a) is an example of a first order (tree-level) B decay, b) are the B^0-$\overline{B^0}$ box diagrams and c) are examples of penguin diagrams mediated by a gluon (QCD penguin) and Z^0/γ (electro-weak penguin).*

3.1 B Mixing in the Standard Model

In the Standard Model, B mixing is dominated by short range interactions described by box diagrams (Particle Data Group 2002). Due to the large top quark mass and the structure of the CKM matrix, the top quark contribution in the loop is dominant. The dispersive part of the B^0-$\overline{B^0}$ oscillation amplitude is calculated to be

$$M_{12}^q = -\frac{G_F^2 m_W^2 \eta_{B_q^0} m_{B_q^0} B_{B_q^0} f_{B_q^0}^2}{12\pi^2} S(m_t^2/m_W^2) \left(V_{tq}^* V_{tb}\right)^2 \tag{60}$$

for quarks $q = d$ or s. G_F, m_W and m_{B_q} are the Fermi coupling constant, W boson mass and the B_q^0 meson mass. The function $S(m_t^2/m_W^2)$ is determined from the ratio of the top and W boson masses, and the QCD correction factor, $\eta_{B_q^0}$, can be calculated reliably with perturbative methods. The B meson decay constant, $f_{B_q^0}$, and the bag parameter $B_{B_q^0}$, have never been measured directly. The most promising theoretical approach to obtain $f_{B_q^0}$ and $B_{B_q^0}$ is through Lattice QCD calculations (Abbaneo 2003).

In calculating the absorptive part of the oscillation amplitude the contribution from the c and u quarks in the loop also needs to be considered,

$$\Gamma_{12}^q = \frac{G_F^2 m_b^2 \eta'_{B_q^0} B_{B_q^0} f_{B_q^0}^2}{8\pi} \left[\left(V_{tq}^* V_{tb} \right)^2 + \frac{8}{3} V_{tq}^* V_{tb} V_{cq}^* V_{cb} \left(\frac{m_c^2}{m_b^2} \right) + \cdots \right]. \tag{61}$$

For both B_d^0 and B_s^0 mesons, we can derive

$$\left| \frac{\Gamma_{12}}{M_{12}} \right| \approx \frac{3\pi}{2} \frac{m_b^2}{m_W^2} \frac{1}{S\left(m_t^2/m_W^2\right)} \approx 5 \times 10^{-3}, \tag{62}$$

which shows that the absorptive part is very small compared to the dispersive part. With this approximation, the mass difference between the two B mass eigenstates, B_H and B_L, can be derived,

$$\Delta M = M_H - M_L = 2|M_{12}| \;\text{ and }\; \Delta\Gamma = \Gamma_L - \Gamma_H = 2|\Gamma_{12}|. \tag{63}$$

Note that, due to the phase difference between M_{12} and Γ_{12}, the heavy mass eigenstate (B_H) decays slower than the light mass eigenstate (B_L).

Using the measured values of $\Delta M = (0.502 \pm 0.006)\,\mathrm{ps}^{-1}$ and the average lifetime $\tau_d = (1.542 \pm 0.016)$ ps, for B_d^0 mesons, it follows that

$$\frac{\Delta\Gamma}{\overline{\Gamma}} \approx 0.5\% \tag{64}$$

and that $\Delta\Gamma$ can be neglected in the B_d^0 system. For the B_s^0 system, only a lower limit of ΔM has been measured to be $14.4\,\mathrm{ps}^{-1}$ with 95% confidence level. Using the measured lifetime, $\tau_s = (1.461 \pm 0.057)$ ps, it follows that

$$\frac{\Delta\Gamma}{\overline{\Gamma}} > 11\%, \tag{65}$$

and the effect of $\Delta\Gamma$ can no longer be neglected in the B_s^0 decay time distributions.

Finally, in the B system, CP violation in the mixing is given by

$$\mathrm{Im}\left\{ \frac{\Gamma_{12}}{M_{12}} \right\} = 1 - \left| \frac{q}{p} \right|^2 \tag{66}$$

$$= -4\pi \frac{m_b^2}{m_W^2} \frac{1}{S(m_t^2/m_W^2)} \mathcal{O}\left(\frac{m_c^2}{m_b^2} \right) \mathrm{Im}\left\{ \frac{V_{tq}^* V_{tb} V_{cq}^* V_{cb}}{|V_{tq}^* V_{tb}|^2} \right\}. \tag{67}$$

Assuming $m_b = 4.25\,\mathrm{GeV/c^2}$, $m_W = 80\,\mathrm{GeVc^2}$ and $m_t = 174\,\mathrm{GeV/c^2}$, this is approximately -6×10^{-4} for B_d^0 and 2×10^{-5} for B_s^0, showing that CP violation in the mixing is small for both the B_d^0 and B_s^0 systems.

3.2 CP Violation in the Standard Model

CP violation in the Standard Model is due to the complex phases of the CKM matrix elements. For example, the $b \to uW$ vertex and its CP conjugate are related by the replacement $V_{ub} \stackrel{\mathrm{CP}}{\to} V_{ub}^*$. For three families of quarks and leptons, 3 angles and 1 complex phase are required to define the CKM matrix. These 4 numbers are fundamental constants of nature, just like the Fermi coupling constant, G_F, or the electromagnetic coupling constant, α_{em}, and need to be determined from experiment.

Hence, the unitary 3×3 CKM matrix can be parameterized by four parameters. One possible choice (Particle Data Group 2002) is to write it in terms of 3 angles, θ_{12}, θ_{23}, θ_{13}, and one complex phase, δ, such that

$$V_{\rm CKM} = R_{23} \times R_{13} \times R_{12}, \tag{68}$$

where

$$R_{12} = \begin{pmatrix} c_{12} & s_{12} & 0 \\ -s_{12} & c_{12} & 0 \\ 0 & 0 & 1 \end{pmatrix} \quad R_{23} = \begin{pmatrix} 1 & 0 & 0 \\ 0 & c_{23} & s_{23} \\ 0 & -s_{23} & c_{23} \end{pmatrix} \quad R_{13} = \begin{pmatrix} c_{13} & 0 & s_{13}e^{-i\delta} \\ 0 & 1 & 0 \\ -s_{13}e^{i\delta} & 0 & c_{13} \end{pmatrix} \tag{69}$$

and $s_{ij} = \sin\theta_{ij}$, $c_{ij} = \cos\theta_{ij}$ and i and j are generation labels.

Another very popular parameterization of the CKM matrix is the perturbative form suggested by Wolfenstein (Wolfenstein 1983) which reflects the hierarchy of the strengths of the quark transitions through charged current interactions as shown in Figure 3. The

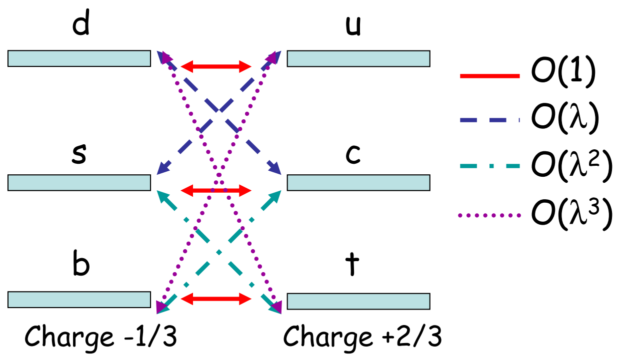

Figure 3. *The hierarchy of quark transitions parameterized by the Wolfenstein parameter* $\lambda \equiv \sin\theta_{12} \sim 0.22$.

Wolfenstein parameterization can be derived by introducing

$$\lambda = s_{12}, \quad A = \frac{s_{23}}{s_{12}^2}, \quad \rho = \frac{s_{13}\cos\delta}{s_{12}s_{23}}, \quad \eta = \frac{s_{13}\sin\delta}{s_{12}s_{23}} \tag{70}$$

where $\lambda \equiv \sin\theta_{12} \sim 0.22$, θ_{12} is the Cabibbo angle and η represents the CP violating phase in the Standard Model. The matrix is expanded in terms of λ and is often approximated to $\mathcal{O}\,(\lambda^3)$,

$$V_{\rm CKM} = \begin{pmatrix} 1-\frac{1}{2}\lambda^2 & \lambda & A\lambda^3(\rho - i\eta) \\ -\lambda & 1-\frac{1}{2}\lambda^2 & A\lambda^2 \\ A\lambda^3(1-\rho-i\eta) & -A\lambda^2 & 1 \end{pmatrix} + \mathcal{O}\left(\lambda^4\right). \tag{71}$$

In the LHC era, next-to-leading order corrections in λ will play an important role and we need to consider the CKM matrix to $\mathcal{O}\left(\lambda^5\right)$,

$$V_{\mathrm{CKM}} = \begin{pmatrix} 1-\frac{1}{2}\lambda^2+\frac{1}{4}\lambda^4 & \lambda & A\lambda^3(\rho-i\eta) \\ -\lambda+\frac{1}{2}A^4\lambda^4-A^2\lambda^5(\rho+i\eta) & 1-\frac{1}{2}\lambda^2+\frac{1}{4}\lambda^4(1-2A^2) & A\lambda^2 \\ A\lambda^3(1-\tilde{\rho}-i\tilde{\eta}) & -A\lambda^2+A\lambda^4\left(\frac{1}{2}-\rho-i\eta\right) & 1-\frac{1}{2}A^2\lambda^4 \end{pmatrix} + \mathcal{O}\left(\lambda^6\right), \tag{72}$$

where $\tilde{\rho}$ and $\tilde{\eta}$ are given by $\tilde{\rho}=\rho(1-\lambda^2/2)$ and $\tilde{\eta}=\eta(1-\lambda^2/2)$.

The requirements for CP violation to be present in the Standard Model can be elegantly summarised by the formula (Jarlskog 1986)

$$\left(m_t^2-m_c^2\right)\left(m_t^2-m_u^2\right)\left(m_c^2-m_u^2\right)\times\left(m_b^2-m_s^2\right)\left(m_b^2-m_d^2\right)\left(m_s^2-m_d^2\right)\times J_{\mathrm{CP}}\neq 0. \tag{73}$$

The first ingredient involves the quark masses and is related to the fact that the CP violating phase could be removed through an appropriate unitary transformation of quark fields, if any 2 quarks of the same charge have equal masses. Consequently, the origin of CP violation is related also to the hierarchy of quark masses. The second ingredient is the Jarlskog determinant, $J_{\mathrm{CP}}=\left|\mathrm{Im}\left\{V_{i\alpha}V_{j\beta}V_{i\beta}^*V_{j\alpha}^*\right\}\right|$, which arises from the unitarity of the CKM matrix and can be interpreted as a measure of the strength of CP violation in the Standard Model. Using the parameterizations of the CKM matrix, J_{CP} can be written as

$$J_{\mathrm{CP}} = s_{12}s_{13}s_{23}c_{12}c_{23}c_{13}\sin\delta = \lambda^6A^2\eta = \mathcal{O}\left(10^{-5}\right) \tag{74}$$

and gives concrete meaning to the fact that CP violation is small in the Standard Model.

3.3 The Unitarity Triangles

The unitarity of the CKM matrix implies that there are six orthogonality conditions between any pair of columns or any pair of rows of the matrix:

$$V_{ud}V_{ub}^*+V_{cd}V_{cb}^*+V_{td}V_{tb}^* = 0 \quad (db) \tag{75}$$
$$V_{us}V_{ub}^*+V_{cs}V_{cb}^*+V_{ts}V_{tb}^* = 0 \quad (sb) \tag{76}$$
$$V_{ud}V_{us}^*+V_{cd}V_{cs}^*+V_{td}V_{ts}^* = 0 \quad (ds) \tag{77}$$

and

$$V_{ud}V_{td}^*+V_{us}V_{ts}^*+V_{ub}V_{tb}^* = 0 \quad (ut) \tag{78}$$
$$V_{cd}V_{td}^*+V_{cs}V_{ts}^*+V_{cb}V_{tb}^* = 0 \quad (ct) \tag{79}$$
$$V_{ud}V_{cd}^*+V_{us}V_{cs}^*+V_{ub}V_{cb}^* = 0 \quad (uc) \tag{80}$$

where the quark pair in parenthesis (ij) represents the condition between the $i'th$ and $j'th$ column or row. Each of the orthogonality conditions requires the sum of three complex numbers to vanish and so can be represented geometrically in the complex plane as a triangle. These are known as the *unitarity triangles* and are shown in Figure 4 using the current experimental values of the various matrix elements $|V_{ij}|$ (Particle Data Group 2002). All six triangles have the same area, equal to $J_{\mathrm{CP}}/2$, which is a measure of CP violation in the Standard Model. It can be seen from Figure 4 that two of the unitarity

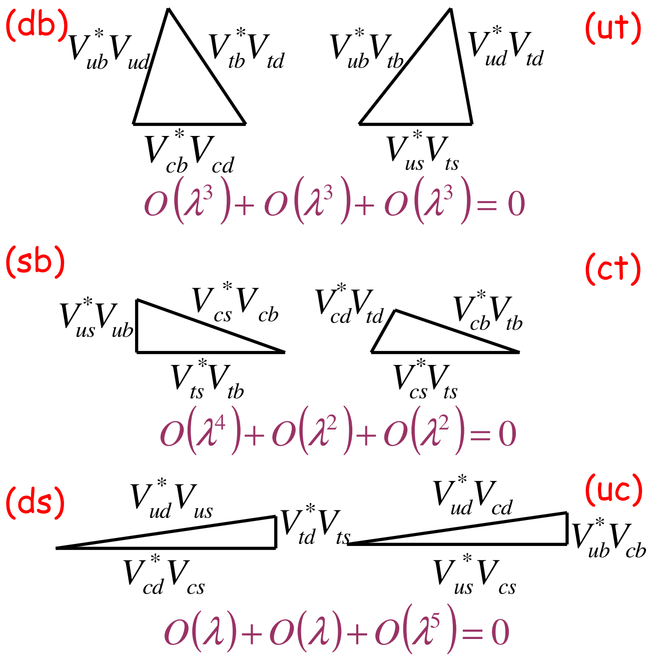

Figure 4. *The six unitarity triangles showing their relative sizes using the current experimental measurements of the CKM matrix elements.*

triangles, (db) and (ut), have all 3 sides of comparable magnitude. These two triangles are redrawn in Figure 5 by choosing a phase convention such that $V_{cd}V_{cb}^*$ is real and dividing the lengths of all the sides by $|V_{cd}V_{cb}^*| = A\lambda^3$. The two triangles are identical to $\mathcal{O}(\lambda^3)$ and differ only by $\mathcal{O}(\lambda^5)$ corrections. The unitarity triangle (db) is commonly referred to as *the* unitarity triangle.

The angles of the triangle (db) are denoted by α, β and γ;

$$\alpha \equiv arg\left(-\frac{V_{td}V_{tb}^*}{V_{ud}V_{ub}^*}\right), \ \beta \equiv arg\left(-\frac{V_{cd}V_{cb}^*}{V_{td}V_{tb}^*}\right), \ \gamma \equiv arg\left(-\frac{V_{ud}V_{ub}^*}{V_{cd}V_{cb}^*}\right), \tag{81}$$

with $\alpha+\beta+\gamma=\pi$. The higher order terms in the CKM matrix introduce a phase in the matrix element V_{ts} such that the relationship between the angles β and γ in the (db) triangle and the angles β' and γ' in the (ut) triangle,

$$\beta' \equiv arg\left(-\frac{V_{ts}V_{us}^*}{V_{td}V_{ud}^*}\right), \ \gamma' \equiv arg\left(-\frac{V_{tb}V_{ub}^*}{V_{ts}V_{us}^*}\right), \tag{82}$$

is given by

$$\beta' = \beta + \chi \ \text{ and } \ \gamma' = \gamma - \chi. \tag{83}$$

The Wolfenstein parameterization of the CKM matrix implies that

$$arg\{V_{td}\} = -\beta, \quad arg\{V_{ub}\} = -\gamma, \quad arg\{V_{ts}\} = \chi + \pi, \tag{84}$$

and that all the other elements are real. Hence, including the angles in the Wolfenstein

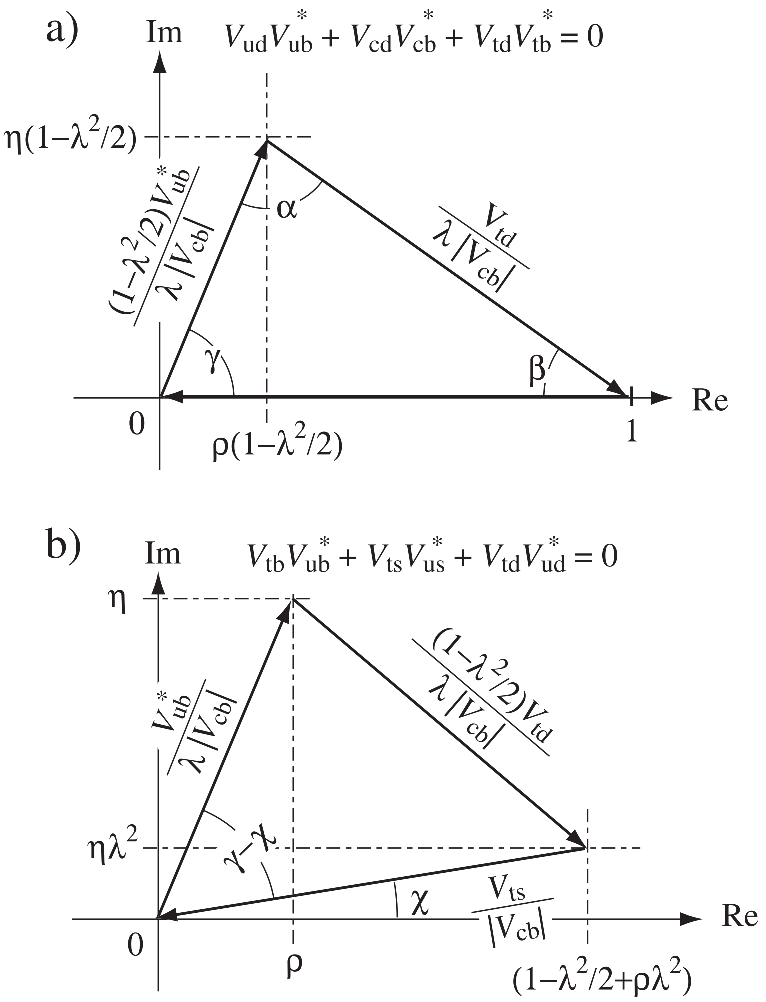

Figure 5. *The unitarity triangles (db) and (ut). The phase convention of the unitarity triangle (db) is chosen such that $V_{cd}V_{cb}^*$ is real and all sides are normalized to $|V_{cd}V_{cb}^*|$.*

parameterization to $\mathcal{O}\ (\lambda^5)$, we find

$$V_{\rm CKM} = \begin{pmatrix} 1-\frac{1}{2}\lambda^2+\frac{1}{4}\lambda^4 & \lambda & -|V_{ub}|e^{-i\gamma} \\ -\lambda+\frac{1}{2}A^4\lambda^4-A^2\lambda^5(\rho+i\eta) & 1-\frac{1}{2}\lambda^2+\frac{1}{4}\lambda^4(1-2A^2) & A\lambda^2 \\ -|V_{td}|e^{-i\beta} & |V_{ts}|e^{-i\chi} & 1-\frac{1}{2}A^2\lambda^4 \end{pmatrix} + \mathcal{O}\left(\lambda^6\right) \tag{85}$$

where β, γ and χ are related to the Wolfenstein parameters λ, ρ and η through

$$\beta = \tan^{-1}\left[\frac{\tilde{\eta}}{1-\tilde{\rho}}\right], \quad \gamma = \tan^{-1}\frac{\eta}{\rho}, \quad \text{and} \quad \chi = \eta\lambda^2. \tag{86}$$

In these lectures, we make allowance for the possibility of new physics beyond the Standard Model description by defining

- *the B_d^0 mixing phase,* $\phi_d = arg\{M_{12}^d\} = 2\beta + \phi_d^{NP}$ and
- *the B_s^0 mixing phase,* $\phi_s = arg\{M_{12}^s\} = -2\chi + \phi_s^{NP}$

where $\phi^{NP}_{d,s}$ is the phase of any new physics in the $B^0 - \overline{B^0}$ box diagrams. We also refer to γ as the *weak decay phase* which can be measured using $b \to u$ transitions but can also be affected by new physics in loop diagrams.

4 B Physics Facilities

Since the b quark was discovered at Fermilab in 1977, many measurements of its confined properties and decay properties have been made at a variety of accelerators and their corresponding experiments. A summary of the parameters of relevant past and present machines is given in Table 1. The design of the experiments and their B physics capabilities are influenced by the different production mechanisms of b quarks which are shown in Figure 6. At high energy hadron colliders, the dominant $b\bar{b}$ production mechanism is expected to be due to gluon fusion processes. At the centre-of-mass energy of the $\Upsilon(4s)$ machines, only B^0_d and $B^\pm$ mesons are produced. At larger centre-of-mass energies, for example at the e^+e^- colliders LEP/SLC and the hadron colliders Tevatron/LHC, all species of B hadrons are produced in the approximate ratio $B^\pm$: B^0_d : B^0_s : b-baryon : $B^\pm_c \approx 39 : 39 : 11 : 12 : 1\%$. In addition, B hadrons are produced with a significant boost, traveling a few millimetres before they decay. A big step therefore in the study of B physics is the deployment of high precision silicon detectors that can reconstruct B decay vertices with an accuracy of a few 10's of μm.

Year	Machine	Energy (GeV)	σ (b)	b fraction	Luminosity ($\mathrm{cm}^{-2}\mathrm{s}^{-1}$)	Total number b pairs ($\times 10^6$)
Symmetric e^+e^- colliders at the $\Upsilon(4s)$						
79-	CESR	10.8	1.05 nb	0.25	1.3×10^{33}	~ 10
73-	DORIS	10.8	1.05 nb	0.23	$\sim 10^{31}$	~ 0.5
Asymmetric e^+e^- colliders at the $\Upsilon(4s)$						
00-	PEP-II	10.8	1.05 nb	0.25	$6.6 \times 10^{33\dagger}$	~ 100
00-	KEK-B	10.8	1.05 nb	0.25	$1.0 \times 10^{34\dagger}$	~ 100
e^+e^- colliders in the continuum						
80-90	PEP	29	0.4 nb	0.09	3.2×10^{31}	
78-86	PETRA	35	0.3 nb	0.09	1.7×10^{31}	
e^+e^- colliders at the Z^0						
89-00	LEP	91	9.2 nb	0.22	2.4×10^{31}	~ 2
89-00	SLC	91	9.2 nb	0.22	3.0×10^{30}	~ 0.09
$p\bar{p}$ hadron colliders						
92-96	Tevatron Run-I	1800	100 μb	0.002	3.0×10^{31}	$5k$ produced
01-	Tevatron Run-II	1960	100 μb	0.002	$1 - 2 \times 10^{32\ddagger}$	

Table 1. *Past and present experimental facilities. † maximum achieved by July 2003. ‡ expected.*

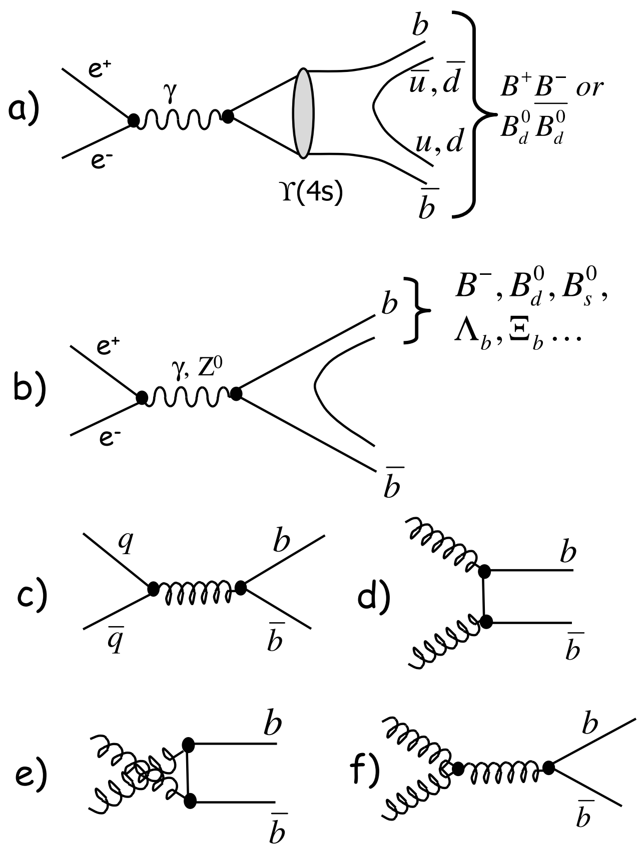

Figure 6. *b quark production mechanisms: a) $e^+e^- \to \Upsilon(4s) \to b\bar{b}$, b) $e^+e^- \to \gamma/Z^0 \to b\bar{b}$, c) and d)-f) are first order $\mathcal{O}(\alpha_s^2)$ quark-quark annihilation and gluon fusion processes respectively.*

Some highlights of B physics over the last 25 years include:

1977 the discovery of the Υ (Fixed target at Fermilab),

1983 the measurement of the inclusive b lifetime (PEP and PETRA),

1984 direct observation of B_d^0 and $B^\pm$ mesons (CLEO and ARGUS),

1987 the observation of B mixing (UA1, ARGUS and CLEO),

1992 evidence for the Λ_b baryon and B_s^0 meson (LEP),

1993 the first observation of $B_d^0 \to K^*\gamma$ and $B_d^0 \to \pi^+\pi^-$ (CLEO),

1994 evidence for the Ξ_b baryon and B^{**} hadrons with non-zero orbital angular momentum (LEP),

1998 the discovery of the $B_c^\pm$ meson (CDF), and

2001 the discovery of CP violation in B_d^0 decays (BaBar and Belle).

By the time LEP and SLC produced their first collisions in 1989, the inclusive b lifetime was known with about a 20% accuracy. The relatively long b lifetime provided the first evidence for a small V_{cb} and the branching ratios of B_d^0 and $B^{\pm}$ decays of $\mathcal{O}(10^{-3})$ had been measured. In recent years, before the start of the B factories, the main contributors to B physics studies have been the e^+e^- colliders operating at the $\Upsilon(4s)$ and at the Z^0 resonance and also the Tevatron $p\bar{p}$ collider. By the start of the 21^{st} century, B physics was promoted to the domain of precision physics.

4.1 BaBar and Belle

In 2000, the PEP-II and KEK-B high luminosity e^+e^- colliders began operation. These machines have separate e^- and e^+ magnet rings so that they can operate at asymmetric energies. The e^+ beam runs at the lower energy of 3.1/3.5GeV (BaBar / Belle) and the e^- beam runs at the higher energy of 9/8GeV (BaBar / Belle). This gives the centre-of-mass of the collision a boost of $\beta\gamma \sim 0.6$ along the beam axis. As a result the decay positions of the two B mesons is typically separated by 250μm. The required luminosity, $\geq 10^{33}\,\mathrm{cm}^{-2}\mathrm{s}^{-1}$, is set by the scale of the branching ratios for B meson decays to the experimentally accessible CP eigenstates, the need to determine the flavour of the other B in the event and the time difference between the two B decays.

The BaBar and Belle detectors, shown in Figure 7, are broadly similar. Each has a silicon vertex detector surrounded by a wire tracking chamber with a helium based gas. They both have particle identification, a CsI(Tl) calorimeter, a superconducting coil and detectors interspersed with iron flux return for K_L^0 and μ identification. BaBar and Belle differ in their choice of silicon detector layout and particle identification. BaBar uses a 5 layer silicon detector with 2 layers at large radii and Belle has a 3 layer silicon detector. Both experiments exploit the dE/dx information in their tracking chambers for particle identification. In addition, BaBar uses long quartz bars to generate Cherenkov light from passing particles and to transport it via total internal reflection to a water-filled torus. Belle uses a combination of TOF and aerogel threshold Cherenkov counters for their particle identification.

The total integrated luminosity collected by Babar and Belle by July 2003 is 130.7 fb^{-1} and 158.7 fb^{-1} respectively (Browder 2003). The peak luminosity at Belle exceeded $10^{34}\,\mathrm{cm}^{-2}\mathrm{s}^{-1}$ in May 2003.

4.2 CDF and D0 Run-II

The Tevatron $p\bar{p}$ collider at Fermilab has undergone a major upgrade since the end of Run-I in 1996. The centre-of-mass energy has been increased to 1.96 TeV with a design luminosity of 5-8 $\times\, 10^{32}\,\mathrm{cm}^{-2}\mathrm{s}^{-1}$ for a final integrated luminosity target of $2\,\mathrm{fb}^{-1}$. Both the CDF and D0 experiments, shown in Figure 8, have undergone major upgrades to operate at high luminosity and shortened bunch spacing (132 ns).

CDF has installed some new components for Run-II, namely a TOF detector to provide hadron particle identification and a hadronic track trigger. The track trigger finds high p_T charged tracks and links them to silicon tracks thereby enabling a cut on the impact parameter to be applied at the trigger level. This is the first time that such a trigger

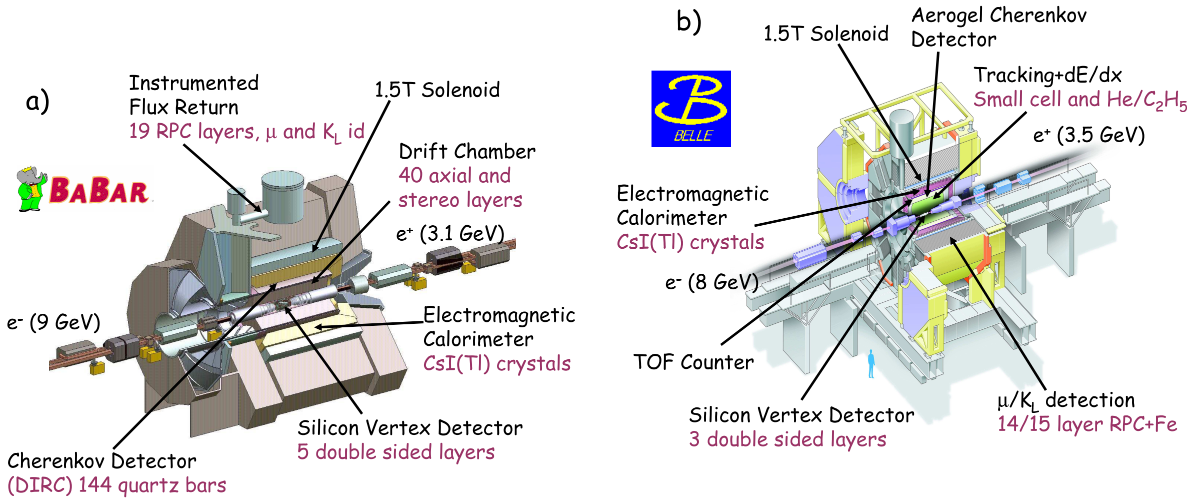

Figure 7. *The BaBar and Belle experiments.*

has been used in a hadron collider environment and is very important for the study of B physics. CDF has also updated the silicon tracker, replaced the tracking system electronics and improved the muon coverage. D0 has installed a 2 T super-conducting magnet, a silicon tracker, a fibre tracker and will also benefit from a silicon track trigger. D0 has also improved its calorimeter readout and upgraded its muon system.

Run-II started in March 2001 and has achieved a peak luminosity of $4.7\times10^{31}\mathrm{cm}^{-2}\mathrm{s}^{-1}$, a factor of 2 below the nominal (Paulini 2003). The main B physics aims of CDF and D0 are to measure the B_s^0 mixing parameter ΔM_s using $B_s^0 \to D_s^{\pm}\pi^{\mp}$ decays, the B_d^0 mixing phase ϕ_d using $B_d^0 \to J/\psi K_S^0$ decays and the weak decay phase γ from a combined analysis of $B_d^0 \to \pi^+\pi^-$ and $B_s^0 \to K^+K^-$ decays before the LHC starts operation.

5 B Physics Experimental Programme

In the CKM picture of the Standard Model with 3 generations there are 4 independent parameters that must be determined from experiment. In the Wolfenstein parameterization these are λ, A, ρ and η. In this section we describe one possible scenario for an experimental programme to determine these four parameters and to over-constrain the Standard Model picture. The theoretical background for this section is described in detail in (Abbaneo 2003) and references therein. Unless otherwise stated, the results quoted are taken from (Schubert 2003).

The parameter λ is determined from precise measurements of $|V_{ud}|$ from nuclear and

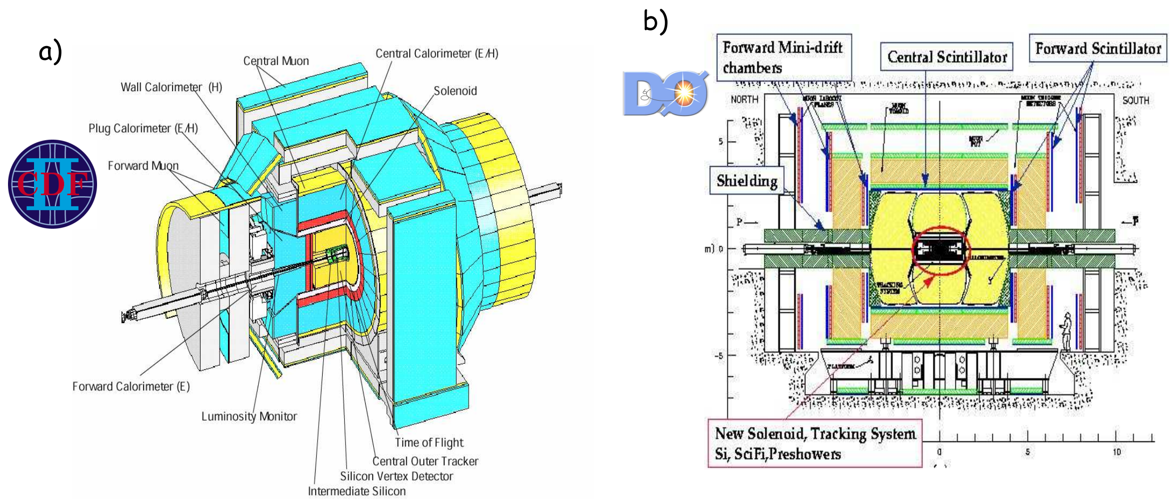

Figure 8. *The CDF and D0 experiments.*

pion beta decay; $|V_{us}|$ from kaon, hyperon and τ decays; $|V_{cd}|$ from ν production of charm quarks; and $|V_{cs}|$ from beta decays of D mesons and decays of real W bosons. The current status from a fit to all the measurements is summarised by

$$\lambda = 0.2235 \pm 0.0033. \tag{87}$$

The remaining 3 parameters are determined from decays of B mesons. The parameter A is determined from the measurement of $|V_{cb}|$ from semi-leptonic B decays. ρ and η are extracted from the current knowledge of the unitarity triangle.

In order to check the internal consistency of the Standard Model picture of the CKM matrix and to search for new physics beyond, a dedicated B physics experimental programme is required. The programme can be sub-divided into 4 stages:

- Stage 1: determine $|V_{ub}|$ and $|V_{cb}|$ from tree-level B decays;
- Stage 2: determine $|V_{td}|$ and $|V_{ts}|$ from loop induced B decays;
- Stage 3: measure the B_d^0 mixing phase from CP violating B decays, thereby checking the consistency of the Standard Model;
- Stage 4: over-constrain the CKM picture and disentangle the new physics and Standard Model contributions using precision measurements of the B_s^0 mixing phase and the weak decay phase.

It is interesting to note that Stages 1 and 2, which give measurements of four CP conserving decays, tell us whether CP violation ($\eta \neq 0$) is predicted in the Standard Model.

5.1 Stage 1: V_{cb} and V_{ub}

The first step has been made by ARGUS and CLEO at the symmetric e^+e^- colliders and the four LEP experiments. BaBar and Belle at the asymmetric e^+e^- colliders are improving the precision on the determinations.

The matrix elements, $|V_{cb}|$ and $|V_{ub}|$, are measured using both inclusive and exclusive semi-leptonic decays of B mesons. Since these are tree-level decays, the values extracted are insensitive to new physics outside of the Standard Model and are therefore universal fundamental constants.

Key rôles in the determination of $|V_{cb}|$ are played by the exclusive decay mode $B_d^0 \to D^*\ell\nu$ and heavy quark effective theory (HQET). HQET is based on the idea that QCD is flavour independent such that, in the limit of infinitely heavy quarks, the quark transition occurs with a unit form factor $\mathcal{F}(1) = 1$ when the quarks are moving with the same invariant four-velocity. Experimentally, the aim is to measure the differential decay rate,

$$\frac{d\Gamma}{d\omega} = \frac{G_F^2}{48\pi^3} K(\omega)\mathcal{F}^2(\omega)|V_{cb}|^2, \tag{88}$$

as a function of ω (the product of the four-velocity of the D^* and the B^0). G_F is the Fermi coupling constant, $K(\omega)$ is a known kinematic factor and $\mathcal{F}(\omega)$ are hadronic form factors. In order to extract $\mathcal{F}(1)|V_{cb}|$, the decay rate is extrapolated to $\omega = 1$ where the D^* is at rest in the B^0 rest frame. To perform this extrapolation, assumptions have to be made about the shape of the form factor $\mathcal{F}(\omega)$. In addition, QCD corrections to $\mathcal{F}(1) = 1$ are required to take into account the effects of the finite mass of the heavy quark. Results obtained from the various QCD approaches yield an average value of

$$\mathcal{F}(1) = 0.91 \pm 0.04, \tag{89}$$

where the error is expected to reduce in the future with progress in unquenched Lattice QCD calculations and improved statistics. The measurement of $|V_{cb}|$ using exclusive decays has been performed by several groups and an example from Belle is shown in Figure 9a) for the reaction $\overline{B^0} \to D^{*+}\ell^-\bar{\nu}$.

An alternative way to determine $|V_{cb}|$ is by comparing the measurement of the semi-leptonic decay width for inclusive $b \to c\ell\nu$ decays to the prediction in the context of the Operator Product Expansion (OPE). Experimentally, the semi-leptonic decay width is determined from the branching ratio and lifetime and is related to $|V_{cb}|$ by

$$\Gamma(B \to X_c\ell\nu) = \frac{Br(B \to X_c\ell\nu)}{\tau_B} = \frac{G_F}{192\pi^3} m_b^5 f\left(\frac{m_c}{m_b}\frac{m_\ell}{m_b}\right)\gamma_c \tag{90}$$

where f is a known phase space factor, depending on the b and c quark masses. γ_c represents the perturbative and non-perturbative corrections which can be expressed using OPE in terms of a double expansion in $1/m_b$ and α_s. At $\mathcal{O}(1/m_b^3)$, the OPE introduces 9 parameters, that can be constrained using measurements of other inclusive kinematic variables, such as the photon energy spectrum in $B \to X_s\gamma$ decays and moments of the lepton and hadronic mass spectra in $B \to X_c\ell\nu$ decays. A comparison of the parameters obtained from the different measurements also provides a consistency test of the theoretical assumptions, notably quark-hadron duality. At the present level of sensitivity, the results show no evidence of any violation effects.

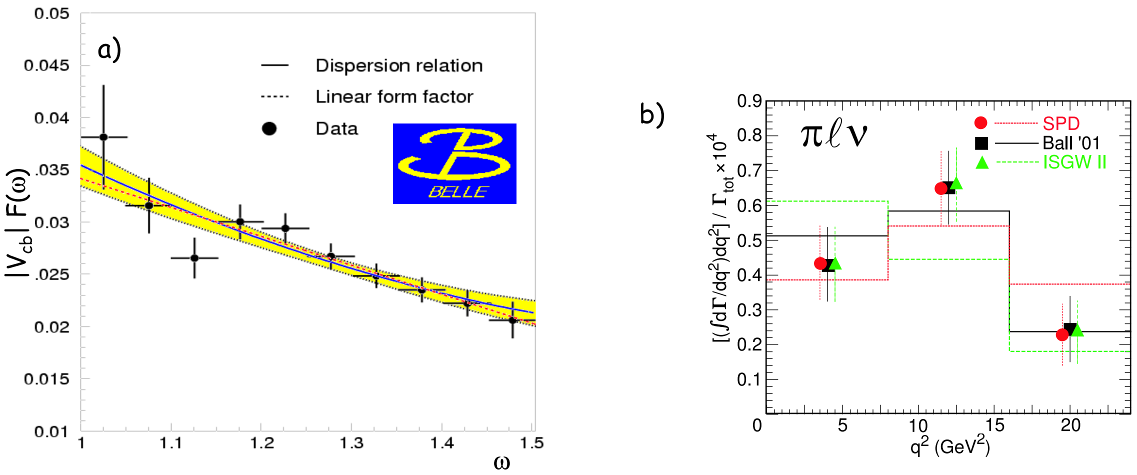

Figure 9. *a) Belle measurement of ω versus $\mathcal{F}(\omega)|V_{cb}|$ using $\overline{B^0} \to D^{*+}\ell^-\bar{\nu}$ decays. b) CLEO measurements of the q^2 distribution for $B \to \pi\ell\nu$ decays compared with various models.*

The present status of the combined exclusive and inclusive measurements of $|V_{cb}|$ is

$$|V_{cb}| = A\lambda^2 = 0.0415 \pm 0.0011. \tag{91}$$

The matrix element $|V_{ub}|$ is determined from semi-leptonic $b \to u\ell\nu$ transitions either through exclusive decays such as $B_d^0 \to \rho, \pi\ell\nu$ or using the event kinematics to separate out the $b \to u$ from the $b \to c$ contributions in inclusive $B \to X\ell\nu$ decays. For the exclusive decays modes, the weak decay involves a heavy to light quark transition so that HQET can not be used directly to extrapolate the form factors. Therefore, the form factors are calculated using a variety of methods based on Lattice QCD, QCD sum rules, perturbative QCD and quark models. At present, none of the methods provides a fully model-independent determination of $|V_{ub}|$. There is also a large spread in the predictions and, in particular, in the q^2 differential distribution. Experimentally, there are two important goals in studying the exclusive charmless semi-leptonic decay modes. The first is to lower the minimum lepton momentum cut and the second is to devise analysis methods that minimize the q^2 dependence of the form factors. A recent CLEO result, uses a low momentum cut of 1.5 GeV and has the feature that the branching fractions are measured in three q^2 intervals. This is shown in Figure 9b) for $b \to \pi\ell\nu$ decays together with the predictions from the various models.

In principle, a clean determination of $|V_{ub}|$ using inclusive semi-leptonic decays can be obtained along same lines as $|V_{cb}|$. However, the main problem here is the large background from $b \to c$ decays. Typical strategies to separate the $b \to u$ from the $b \to c$ contributions involve applying severe kinematic cuts which significantly restrict the available phase space and exaggerate the theoretical errors. The three main cuts that have been used by the experiments include a cut on the lepton momentum, a cut on the hadronic invariant mass and a cut on the leptonic invariant mass. A reduction in the theoretical uncertainties can be achieved by using more complex kinematic cuts or, by measuring the universal structure function, which describes the distribution of the light-cone component of the residual momentum of the b quark, in some other process, such as the γ spectrum in $b \to s\gamma$ decays.

The present status of the combined exclusive and inclusive measurements of $|V_{ub}|$ is

$$|V_{ub}| = (3.80^{+0.24}_{-0.13} \pm 0.45) \times 10^{-3}. \tag{92}$$

5.2 Stage 2: V_{td} and V_{ts}

The matrix elements $|V_{td}|$ and $|V_{ts}|$ are extracted from the measurement of ΔM defined by equations (60) and (63) using a fit to the mixing asymmetry,

$$\mathcal{A}_{mix} = \frac{P(B^0 \to B^0) - P(B^0 \to \overline{B^0})}{P(B^0 \to B^0) + P(B^0 \to \overline{B^0})} = \cos \Delta M t \tag{93}$$

or fraction of mixed events,

$$\mathcal{F}_{mix} = \frac{P(B^0 \to \overline{B^0})}{P(B^0 \to B^0) + P(B^0 \to \overline{B^0})} = \frac{(1 - \cos \Delta M t)}{2} \tag{94}$$

using many different analysis methods. Experimentally, these measurements require the knowledge of the proper time of the B^0 and the flavour of the B^0 or $\overline{B^0}$ at production and decay. The extraction of $|V_{td}|$ or $|V_{ts}|$ requires the knowledge of the weak decay constant, f_{B_q}, and the bag parameter, B_{B_q}. Recent QCD sum rules and partially quenched Lattice calculations give

$$f_{B_d}\sqrt{B_{B_d}} = 223 \pm 33 \pm 12\,\mathrm{MeV} \quad \text{and} \quad \xi = \frac{f_{B_s}\sqrt{B_{B_s}}}{f_{B_d}\sqrt{B_{B_d}}} = 1.24 \pm 0.04 \pm 0.06. \tag{95}$$

Examples of the fits for ΔM_d are shown in Figure 10. The current world average value for ΔM_d (HFAG 2003) is

$$\Delta M_d = (0.502 \pm 0.006)\,\mathrm{ps}^{-1} \tag{96}$$

and translates into

$$|V_{td}||V_{tb}| = (9.2 \pm 1.4 \pm 0.5) \times 10^{-3}. \tag{97}$$

No B_s^0 oscillation signal has yet been observed. However, a limit is placed on the B_s^0 oscillation frequency using an *amplitude* method. This is illustrated in Figure 10 where the world average of all the B_s^0 oscillation measurements are presented. The current limit on ΔM_s is given by

$$\Delta M_s > 14.4\mathrm{ps}^{-1} \tag{98}$$

giving

$$|V_{ts}||V_{tb}| > 0.033. \tag{99}$$

Alternatively, $|V_{ts}|$ can be extracted from a measurement of the branching fraction of $b \to s\gamma$ decays. The present measurements result in

$$|V_{ts}||V_{tb}| = 0.047 \pm 0.008. \tag{100}$$

CDF is also making progress in the measurement of B_s^0 mixing using the exclusive decay mode $B_s^0 \to D_s^{\pm}\pi^{\mp}$ (Harr 2003). They currently have 84 ± 11 signal events from an integrated luminosity of 119 pb^{-1}, reconstructed using the $D_s^{\pm} \to \phi\pi^{\pm}$ decay channel. The B_s^0 invariant mass spectrum is shown in Figure 11. However, in order to observe Standard Model B_s^0 oscillations ($\Delta M_s \sim 20\text{ps}^{-1}$) at the 5σ level, they need a ten-fold increase in statistics.

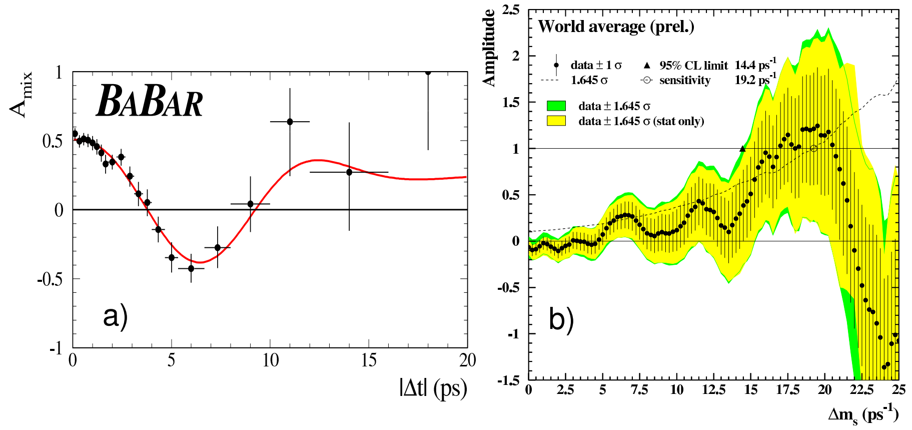

Figure 10. *a) An example of the ΔM_d fit to the mixing asymmetry $\mathcal{A}_{mix}$ using fully reconstructed $B_d^0 \to \overline{D}^{(*)}X$ events from BaBar (BaBar 2002) and b) the combined measurements of the B_s^0 oscillation amplitude as a function of ΔM_s (HFAG 2003).*

5.3 Stage 3: The B_d^0 Mixing Phase

In the Standard Model, the B_d^0 mixing phase, ϕ_d, is given by the CKM angle β and is an example of CP violation in the interference which can be measured using the CP asymmetry given in equation (41). The *golden* decay channel for this measurement, $B_d^0 \to J/\psi K_S^0$, is dominated by the tree level Feynman diagram. The weak phase of the penguin contribution, $arg\{V_{ts}V_{tb}^*\}$ is similar to the weak phase of the tree decay but does not affect the parameter λ defined in equation (24). However, the effect of K^0-$\overline{K^0}$ mixing has to be taken into account and therefore

$$\begin{aligned}\lambda(B_d^0 \to J/\psi K_S^0) &= \left(\frac{q}{p}\right)_{B_d^0}\left(\frac{q}{p}\right)_{K^0}\left(\frac{\overline{A}}{A}\right)_{J/\psi K_S^0} \\ &= -\left(\frac{V_{tb}^*V_{td}}{V_{tb}V_{td}^*}\right)\left(\frac{V_{cs}V_{cd}^*}{V_{cs}^*V_{cd}}\right)\left(\frac{V_{cb}V_{cs}^*}{V_{cb}^*V_{cs}}\right)\end{aligned} \tag{101}$$

where the minus sign takes into account that $J/\psi K_S^0$ is a CP odd state, and leads to

$$\mathrm{Im}\,\{\lambda(B_d^0 \to J/\psi K_S^0)\} = \mathrm{Im}\,\{-e^{-2i\beta}\} = \sin 2\beta. \tag{102}$$

The measurement of the B_d^0 mixing phase has recently been performed by the B factory experiments, BaBar and Belle , using the decay channel $B_d^0 \to J/\psi K_S^0$. The

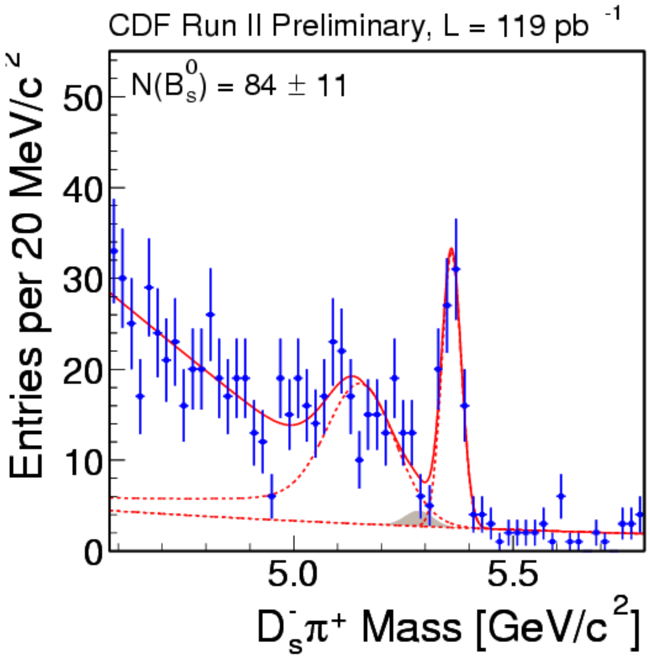

Figure 11. *The $D_s^{\pm}\pi^{\mp}$ candidate mass spectrum for $D_s^{\pm} \rightarrow \phi\pi^{\pm}$ from CDF. The curve is a fit to the signal shapes for $\overline{B_s^0} \rightarrow D_s^+\pi^-$ (narrow peak) and $\overline{B_s^0} \rightarrow D_s^{*+}\pi^-$ (wide peak), where the photon from the D_s^{*+} decay is not observed.*

experimental determination of the CP asymmetry and hence the B_d^0 mixing phase involves 3 key elements. Firstly, the $J/\psi K_S^0$ final state needs to be reconstructed, which requires good momentum and energy resolution for charged particles. Secondly, the determination of the b quark flavour requires good particle identification to identify kaons and leptons. Finally, the decay time difference between the $B_d^0 \rightarrow J/\psi K_S^0$ and the other B needs to be computed. This requires excellent vertex resolution to measure distance. A measurement of the CP asymmetry for $B_d^0 \rightarrow J/\psi K_S^0$ and other charmonium/K^0 decays from Belle is shown in Figure 12. The latest results presented by BaBar and Belle (Browder 2003) are

$$\sin\phi_d = 0.741 \pm 0.067 \pm 0.033 \quad \text{BaBar} \quad 81\,\text{fb}^{-1} \tag{103}$$

$$\sin\phi_d = 0.733 \pm 0.057 \pm 0.028 \quad \text{Belle} \quad 140\,\text{fb}^{-1} \tag{104}$$

$$\sin\phi_d = 0.736 \pm 0.049 \quad \text{Average} \tag{105}$$

where ϕ_d is identical to 2β if only Standard Model box processes contribute to B_d^0 oscillations. The average value for this direct measurement of $\sin\phi_d$ can be compared to the prediction of $\sin 2\beta$ obtained from the currently known values of $|V_{cb}|$, $|V_{ub}|$, $|V_{td}|$ and $|V_{ts}|$,

$$\sin 2\beta_{side} = 0.695 \pm 0.055. \tag{106}$$

This shows that the Standard Model currently gives a very consistent picture.

The current status of the unitarity triangle is summarised in Figure 13. The measure-

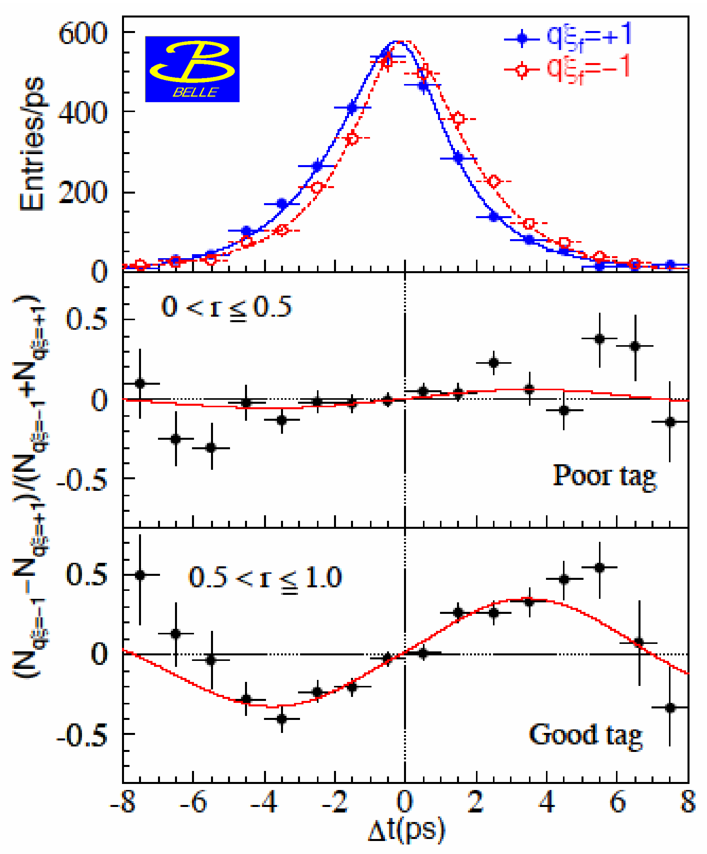

Figure 12. *The Belle proper time distribution for events with a tagged B_d^0 (open circles) and $\overline{B_d^0}$ (closed circles) meson in the event for $B_d^0 \to J/\psi K_S^0$ decays and other charmonium/K_S^0 final states. Also shown is the CP asymmetry for poor and good tags.*

ments of $|V_{ub}|$ and $|V_{cb}|$ are related to ρ and η through

$$\sqrt{\tilde{\rho}^2 + \tilde{\eta}^2} = \left(1 - \frac{\lambda^2}{2}\right) \frac{1}{\lambda} \left|\frac{V_{ub}}{V_{cb}}\right| \qquad (107)$$

and result in a circular band centered on $(\tilde{\rho}, \tilde{\eta}) = (0, 0)$. The measurement of $|V_{td}|$ and the limit on $|V_{ts}|$ are related to ρ and η through

$$\sqrt{(1 - \tilde{\rho})^2 + \tilde{\eta}^2} = \frac{1}{\lambda} \left|\frac{V_{td}}{V_{cb}}\right| \approx \frac{1}{\lambda} \left|\frac{V_{td}}{V_{ts}}\right| \qquad (108)$$

and result in a circular band centered on $(\tilde{\rho}, \tilde{\eta}) = (1, 0)$. The direct measurement of $\sin \phi_d$ is related to ρ and η via equation (86) when interpreted in terms of the Standard Model. The best fit to these B physics results, together with the measurement of $\varepsilon \propto \tilde{\eta}(1 - \tilde{\rho})$ from kaon decays, gives

$$\tilde{\rho} = 0.21 \pm 0.08 \pm 0.05 \qquad (109)$$

$$\tilde{\eta} = 0.34 \pm 0.04 \pm 0.02 \qquad (110)$$

and is consistent with CP violation in the Standard Model.

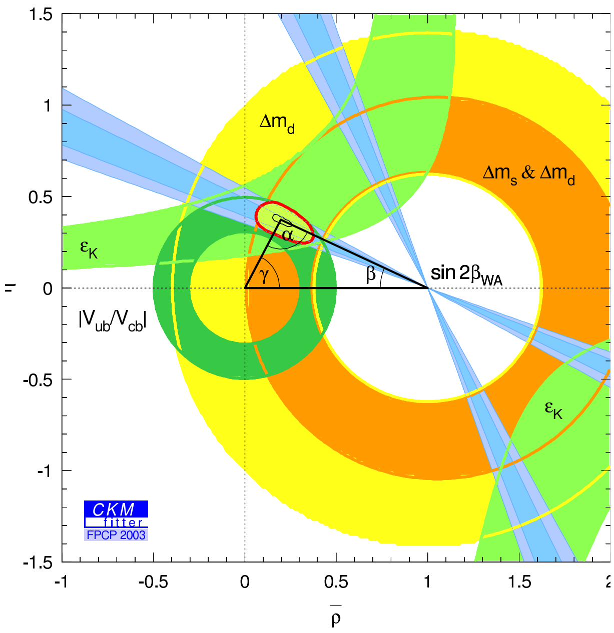

Figure 13. *The current status of the unitarity triangle from constraints on $\tilde{\rho}$ and $\tilde{\eta}$ using the values of $|V_{ub}|$, $|V_{cb}|$, the measurement of B_d^0 mixing, the upper limit on B_s^0 mixing, the measurement of the B_d^0 mixing phase and ε from kaon decays (Charles 2003).*

5.4 Stage 4: Future

A fully comprehensive study of CP violation that includes the separation of possible new physics contributions from those of the Standard Model requires ultra-high statistics for B meson decays and the availability of the B_s^0 meson. This will be carried out by the next generation of B physics experiments and are the subject of the remainder of these lectures.

6 Next Generation B Physics Experiments

The main B physics aims of the next generation of experiments, namely the dedicated B physics experiments, LHCb at the LHC and the BTeV experiment at the Tevatron collider, as well as the general purpose experiments ATLAS and CMS at the LHC, are

- to make precise measurements of CKM parameters with small model dependence;
- to search for new physics via CP violating phases; and
- to search for new physics via rare decays;

as well as covering a broad program of heavy flavour physics. A summary of the running parameters of the LHC and Tevatron colliders and experiments are given in Table 2. The main advantages of studying B physics at hadron colliders compared to e^+e^- colliders are

- a large $b\bar{b}$ cross-section, $\sigma_{b\bar{b}} \sim$ 100-500 μb for $\sqrt{s}$ = 2-14 TeV, corresponding to 10^{11}-10^{12} $b\bar{b}$ produced per year at a luminosity of $2 \times 10^{32}\,\mathrm{cm}^{-2}\mathrm{s}^{-1}$;
- the production of all species of B hadrons ($B^{\pm}$, B^0_d, B^0_s, $B^{\pm}_c$ and b-baryons); and
- a large number of primary particles to determine the b production vertex.

An experimental difficulty arises from the large inelastic cross-section, $\sigma_{b\bar{b}}/\sigma_{inelastic} \sim$ 0.2-0.6% for $\sqrt{s}$ = 2-14 TeV. The hadron collider experiments therefore require excellent triggering capabilities to reduce the minimum-bias background. The main disadvantages for performing B physics studies at hadron colliders are that many particles are produced which are not associated with B hadrons; and that the B hadrons do not evolve coherently and hence B^0 mixing dilutes the flavour tagging.

	Tevatron	LHC	
Energy/collision mode	2.0 TeV $p\bar{p}$	14.0 TeV pp	
$b\bar{b}$ cross-section	$\sim 100\mu$b	$\sim 500\mu$b	
Inelastic cross-section	$\sim$ 50mb	$\sim$ 80mb	
Ratio $b\bar{b}$/inelastic	0.2%	0.6%	
Bunch spacing	132 ns	25 ns	
Bunch length	$\sim$ 30cm	$\sim$ 5cm	
	BTeV	LHCb	ATLAS / CMS
Status	Pending finance	In construction	In construction
Start date	2009	2007	2007
Detector configuration	Single-arm forward	Single-arm forward	Central detector
Running luminosity	$2 \times 10^{32}\,\mathrm{cm}^{-2}\mathrm{s}^{-1}$	$2 \times 10^{32}\,\mathrm{cm}^{-2}\mathrm{s}^{-1}$	$1 \times 10^{33}\,\mathrm{cm}^{-2}\mathrm{s}^{-1}\,(10^{34})$
$b\bar{b}$ events per 10^7 sec	$2 \times 10^{11} \times accep$	$1 \times 10^{12} \times accep$	$5 \times 10^{12} \times accep$
$\langle$Interactions/crossing$\rangle$	$\sim$ 1.6	$\sim$ 0.5 (30% single int.)	$\sim$ 2.3 (20)

Table 2. *Comparison of the LHC and Tevatron collider running parameters and experiments.*

The dedicated B experiments, LHCb and BTeV, take full advantage of a forward detector geometry which is based on the fact that both the b- and $\bar{b}$-hadrons are predominantly produced in the same forward (or backward) direction at high energies. This is demonstrated in Figure 14 where the polar angles of the b- and $\bar{b}$-hadrons are shown in events generated with the PYTHIA simulation programme. The polar angle is defined with respect to the beam axis in the pp centre-of-mass system. Detecting both b- and $\bar{b}$-hadron at the same time is essential for the flavour tag. Further advantages of a forward geometry are

- The b-hadrons produced are faster than those in the central region. Their average momentum is about 80 GeV/c, corresponding to a mean decay length of $\sim$7mm. Therefore, a good decay time resolution can be obtained for reconstructed B-mesons.

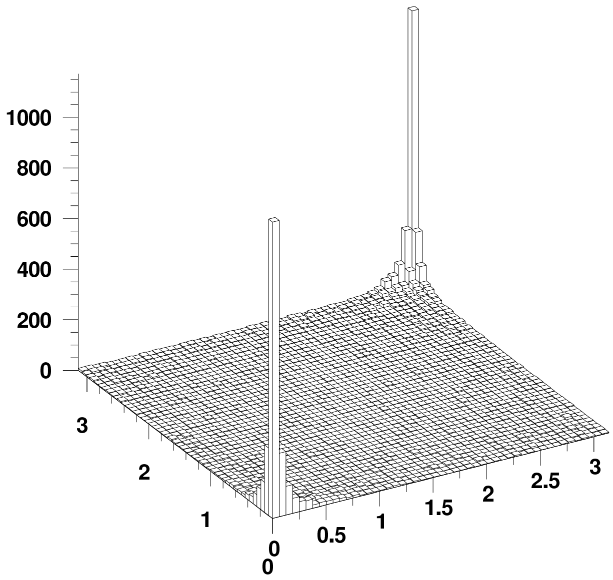

Figure 14. *Polar angles of the b- and $\overline{b}$-hadrons*

- The spectrometer can be built in an open geometry with an interaction region which is not surrounded by all the detector elements. This allows the vertex detector system to be built with sensors that can be moved away from the beam during injection. During data taking, the sensors are positioned closer to the beam in order to achieve a good vertex resolution.
- In the forward region, momenta are mainly carried by the longitudinal components. Therefore, the threshold value for the p_t trigger can be set low for electrons, muons and hadrons without being constrained by the detector requirements. This makes the p_t trigger more efficient than in the central region.
- The momentum range required for particle identification is well matched to Ring Imaging Cherenkov detectors.
- The open geometry allows easy installation, maintenance and possible upgrades.

A disadvantage of the forward geometry is that the minimum-bias background also peaks forward resulting in high occupancy and high track density and therefore requiring a finer segmentation of the detector components. Both LHCb and BTeV choose to run at a luminosity of $2 \times 10^{32}\,\mathrm{cm}^{-2}\mathrm{s}^{-1}$. This optimal luminosity is chosen in a region where one inelastic interaction per bunch crossing dominates simplifying the event reconstruction and reducing radiation levels.

In order to exploit the full potential of the LHC, the experiments require the following capabilities

- a trigger sensitive to both leptonic and hadronic final states;
- a particle identification system capable of identifying p, K, π, μ and e within the required momentum range;
- a vertex detector able to reconstruct primary and B vertices very precisely;

- a tracking system with good momentum resolution; and
- an electromagnetic calorimeter capable of reconstructing π^0 decays.

We will now discuss to what extent each of the experiments matches these requirements.

6.1 LHCb

The LHCb experiment (Amato 1998) is a single-arm forward spectrometer designed to run at a lower luminosity ($2 \times 10^{32}\,\mathrm{cm}^{-2}\mathrm{s}^{-1}$) than the nominal LHC luminosity ($10^{34}\,\mathrm{cm}^{-2}\mathrm{s}^{-1}$) and will perform its full physics programme from the start of LHC operation. The detector layout, recently optimized to reduce the material budget of the experiment and to improve the trigger performance (Antunes Nobrega 2003), is shown in Figure 15. It consists of the beam-pipe, a silicon strip Vertex Locator (VELO), a dipole magnet, a tracking system, two Ring Imaging Cherenkov detectors with three radiators, a calorimeter system and muon system. The pp interaction point is contained within the VELO detector and the 1.1 T dipole magnet is displaced ~ 5 metres upstream. The LHCb trigger is designed to distinguish minimum-bias events from events containing B hadrons through the presence of particles with a large transverse momentum p_T and the existence of secondary vertices. The fringe field from the magnet, in the region between the VELO and RICH-1, is used to provide p_T information for tracks with large impact parameter.

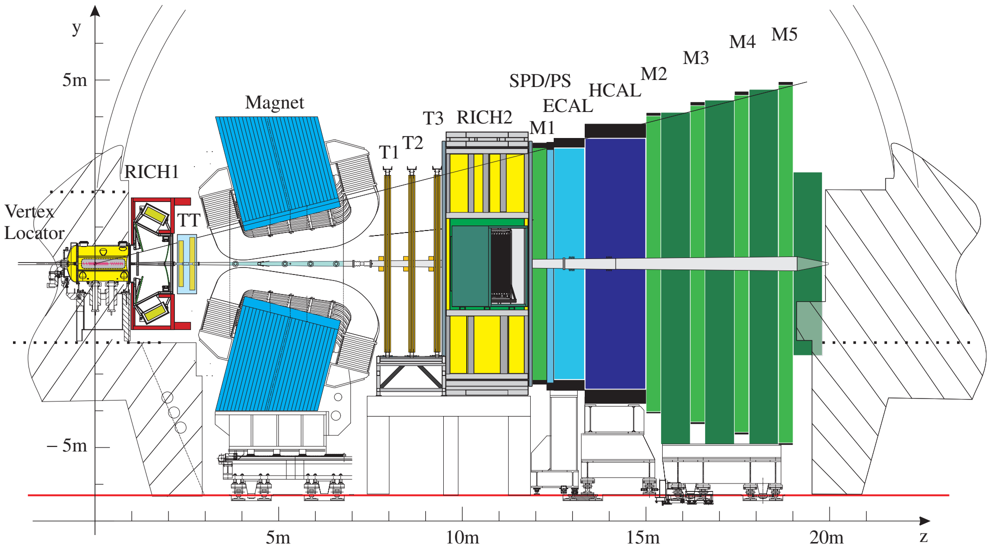

Figure 15. *The LHCb experiment.*

6.2 BTeV

BTeV is a single-arm forward spectrometer (Drobychev 2002), shown in Figure 16, and will run at the Tevatron $p\bar{p}$ collider from 2009. A key design feature of BTeV is the silicon pixel detector, which is centered on the interaction region and surrounded by a 1.5 T magnet. The main advantages of using a silicon pixel detector compared to a silicon strip detector are a better signal to noise ratio, a 5-10 μm spatial resolution, a lower occupancy and radiation hardness. The main disadvantages are the large radiation length ($\sim 1X_0$) and the number of readout channels. A unique feature of the BTeV silicon pixel detector is that it will be used in the lowest level trigger system. Other features of the experiment include a tracking system, a single RICH detector with 2 radiators, a lead-tungstate calorimeter and a muon detector.

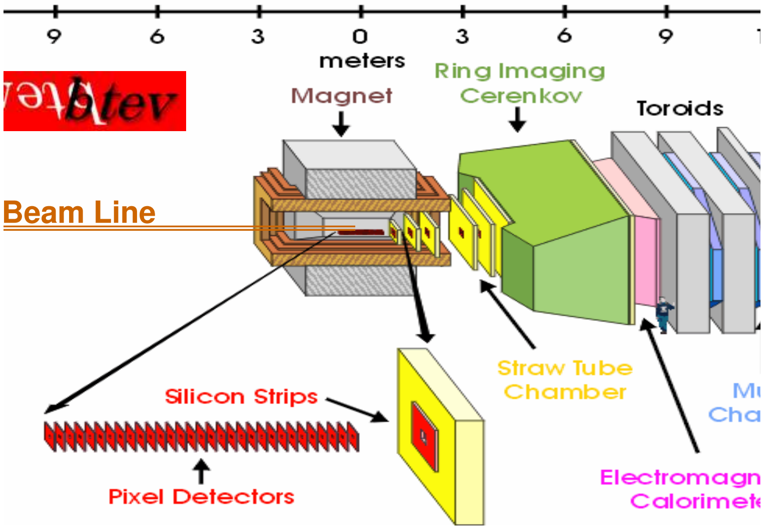

Figure 16. *The BTeV experiment.*

6.3 ATLAS and CMS

ATLAS and CMS are general purpose collider detectors designed to perform high p_T physics at the LHC (Virdee 2003). During the first three years of running, the LHC will operate at a low luminosity, $1 \times 10^{33}\,\mathrm{cm}^{-2}\mathrm{s}^{-1}$, enabling ATLAS and CMS to pursue a B physics programme. The B capabilities of the experiments are achieved through the employment of silicon pixel and microstrip detectors and specialist B triggers by reducing the lepton p_T thresholds to a minimum. Both ATLAS and CMS have excellent muon and electron detection capabilities, and a good vertex resolution, allowing them to collect a high statistics sample of decays such as $J/\psi K_S^0$ and $J/\psi\phi$. However, their first level high p_T lepton trigger is insensitive to purely hadronic final states, which can only be triggered by the presence of a semi-leptonic decay of the other b quark. The two experiments also have no $p/K/\pi$ separation capability in the relevant momentum range, although the energy loss, dE/dx, can be used for particle identification at low momenta. In particular, they cannot separate kaons from pions in the high momentum region relevant for two-body decay modes of B mesons such as $\pi^+\pi^-$ and D_sK. For these reasons, it is not expected that ATLAS and CMS will be able to study CP violation with all the final states necessary to perform a model-independent analysis. They will, however, have a large acceptance for very rare B decays, such as $B \to \mu^+\mu^-$.

7 B Physics at the LHC

7.1 B Production

The physics of generic B production (Ahmadov 2000) enters in many ways in the context of B physics in the LHC era. It affects the possibilities of B decay studies, it can be used for QCD tests and is an important background for several processes of interest. B production at hadron colliders was first observed by UA1 at the $Sp\bar{p}S$ and has subsequently been studied at the Tevatron collider. Studies include the shape of the p_T distribution for b production and the correlations between the b and $\bar{b}$. Phenomenologically, these are reasonably well explained by next-to-leading order QCD (NLO QCD). However, the observed b production cross-section measured at the Tevatron is larger than expected and is underestimated by a factor of ~ 2.4. There are 3 possible explanations for this discrepancy (Salam 2002). The first explanation is that the absolute normalisation of the cross-section is not correctly predicted due to the possible presence of large higher order terms (NNLO QCD). The second explanation is that the shape of the p_T distribution is distorted by some perturbative or non-perturbative effects, such as fragmentation. Finally, it has been suggested that the discrepancy could be due to the production of light gluinos with a mass of $\sim 14\,\text{GeV}$. Studies of generic B production physics are under investigation by the next generation experiments. One example is the study by ATLAS of $b\bar{b}$ production correlations using the J/ψ from exclusive $B_d^0 \to J/\psi K_S^0$ or $B_s^0 \to J/\psi\phi$ decays and the muon from the semi-leptonic decay of the other B in the event (Ohlsson-Malek 2003).

The physics of B production can also be interpreted as the study of the production and properties, e.g. mass and lifetime, of the individual B species. For example, a copious number of $B_c^\pm$ mesons, $\sim 10^9$, will be produced at the LHC in one year of running. A study by the LHCb experiment of the decay mode $B_c^\pm \to J/\psi\pi^\pm$, which has an expected visible branching ratio of 6.8×10^{-4}, results in an annual yield of 14k events with a background to signal ratio of < 0.8 (Antunes Nobrega 2003). The $B_c^\pm$ meson can also be used for CP violation studies, for example in the decay modes $B_c^\pm \to J/\psi D^\pm$ and $B_c^\pm \to D_s^\pm D^0$, although several years of running will be required to provide sufficient statistics.

7.2 B Decay

We now turn our attention to the study of CP violation and the search for new physics in B decays in the LHC era. We start by considering a few examples of how the B_s^0 mixing frequency ΔM_s, the B_d^0 mixing phase ϕ_d, the B_s^0 mixing phase ϕ_s, and the weak decay phase γ can be measured at the LHC. The CKM angle α is notoriously difficult to measure, mainly because the decay mode $B_d^0 \to \pi^+\pi^-$ is plagued by large penguin contributions, and will not be discussed here. For the sake of clarity, we also will restrict our discussions to the recent studies performed by the LHCb experiment (Antunes Nobrega 2003). We will then discuss the interpretation of these measurements in the presence of new physics and how the contributions from new physics and the Standard Model can be separated. Finally, we will review the physics of very rare B decay modes.

B decays can be subdivided into three main categories, neutral (B_d^0, B_s^0) decays, charged ($B^{\pm}$, $B_c^{\pm}$) decays and decays of b-baryons (Λ_b, Ξ_b etc). Here, we shall focus on the physics of neutral B decays, which can be further categorized according to their final state:

- flavour specific final state
- flavour non-specific final state, of which there are
  - CP eigenstates
  - mixed CP eigenstates and
  - non-CP eigenstates.

At the LHC, the measurement of ΔM_s is studied using a flavour-specific final state whereas the study of CP violation uses all types of flavour non-specific final states. The B decay modes that will be discussed in these lectures and the CKM parameters they probe are shown in Figure 17.

7.2.1 B_s^0 Mixing

At the LHC, the B_s^0 mixing frequency will be measured using the $B_s^0 \to D_s^{\pm}\pi^{\mp}$ decay channel, which has a large visible branching ratio ($\mathrm{Br}(B_s^0 \to D_s^{\pm}\pi^{\mp}) = 120 \times 10^{-6}$) and is an example of a flavour-specific final state in which only a single tree diagram contributes. It is therefore considered as a *gold-plated* channel for the study of B_s^0 mixing. The generic decay formulae, equations (20) and (21), can be applied with the constraint $\lambda = 0$ ($|q/p| = 1$) and a flavour asymmetry can be defined,

$$\mathcal{A}_{flav} = \frac{\Gamma_{\overline{B}\to f} - \Gamma_{B\to f}}{\Gamma_{\overline{B}\to f} + \Gamma_{B\to f}} = -D\frac{\cos\Delta M_s t}{\cosh\Delta\Gamma_s t} \tag{111}$$

where D is a dilution factor due to wrong tagging and experimental resolution. From this asymmetry, the B_s^0 oscillation frequency ΔM_s and, optionally, the decay width difference $\Delta\Gamma_s$ can be determined.

A study of B_s^0 mixing by LHCb using $B_s^0 \to D_s^{\pm}\pi^{\mp}$ decays where the D_s is fully reconstructed in the $D_s^{\pm} \to K^+K^-\pi^{\pm}$ final state has recently been performed. The analysis benefits from excellent mass (14 MeV) and decay time (44 fs) resolutions. The expected $B_s^0 \to D_s^{\pm}\pi^{\mp}$ decay rate as a function of proper time t for two different values of ΔM_s is shown in Figure 18. The expected ΔM_s sensitivity for one year of data taking is $\sim 0.01\,\mathrm{ps}^{-1}$ and results in a $> 5\sigma$ measurement up to values of $\Delta M_s = 68\,\mathrm{ps}^{-1}$. The equivalent sensitivities for ATLAS and CMS are $36\,\mathrm{ps}^{-1}$ and $30\,\mathrm{ps}^{-1}$ respectively (Ohlsson-Malek 2003).

7.2.2 The B_d^0 Mixing Phase

We have already discussed the extraction of the B_d^0 mixing phase, in the context of the current generation of experiments (see Section 5.3). At the LHC, the *gold-plated* decay mode $B_d^0 \to J/\psi K_S^0$, an example of a flavour non-specific CP eigenstate, will be also

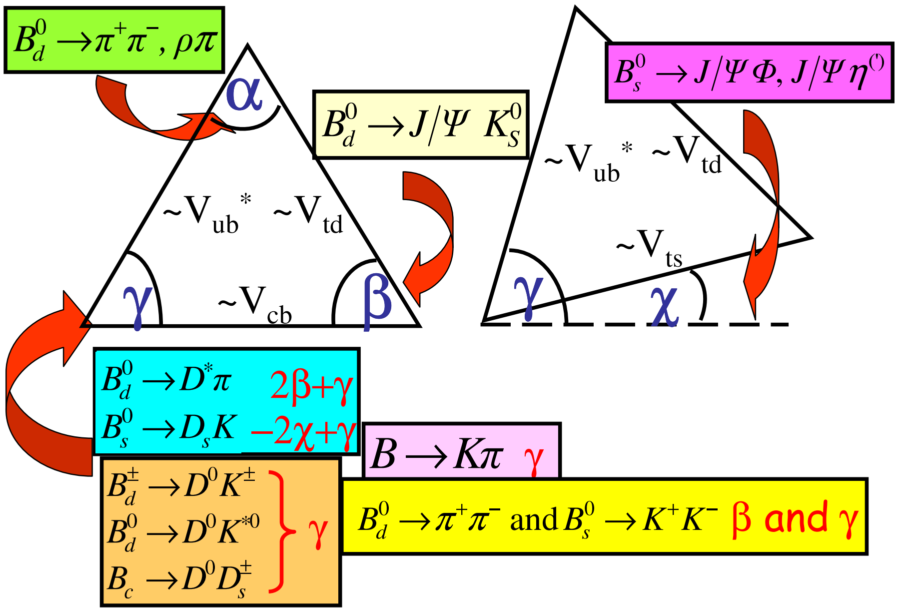

Figure 17. *A summary of the B decay modes and the relevant CKM phases they probe discussed in these lectures.*

central to the measurement of the B_d^0 mixing phase. The current results from the B factory experiments are consistent with the Standard Model expectations, $\mathcal{A}^{dir} = 0$ (i.e. $|\lambda| = 1$) and $\mathcal{A}^{mix} = \mathrm{Im}\{\lambda\} = \sin 2\beta$. However, precision measurements are important as new physics could affect these parameters at the level of precision reached in the LHC era. In addition, we shall see in Section 7.2.4 that a precise measurement of ϕ_d is required for the extraction of the weak decay phase γ from analyses such as the combined study of the $B_d^0 \to \pi^+\pi^-$ and $B_s^0 \to K^+K^-$ decay modes. An example of a fit to the $B_d^0 \to J/\psi K_S^0$ CP asymmetry is shown in Figure 19. The statistical sensitivities on the parameters $\sin\phi_d$ and $|\lambda|$ expected in one year of data taking are 0.022 and 0.023 respectively. In 5 years at the LHC, the expected precision of $\sin\phi_d$ using all the data from LHCb, ATLAS and CMS is expected to reach 0.005.

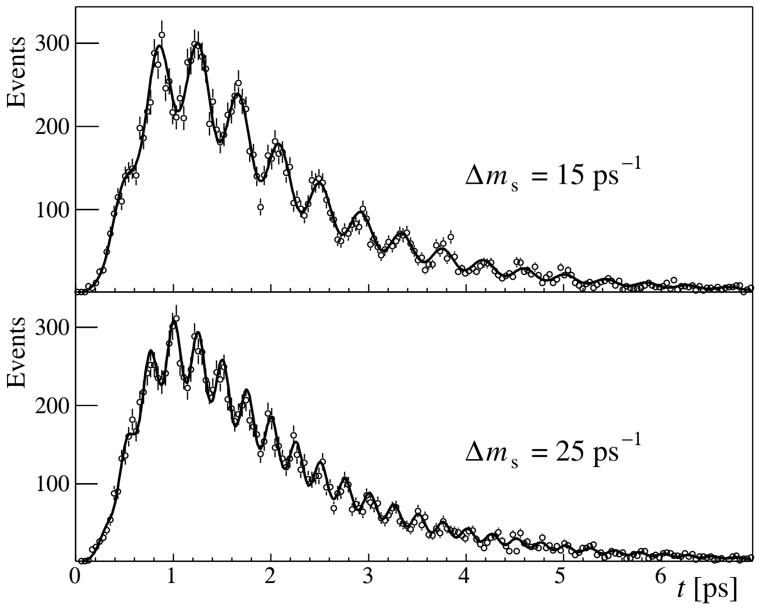

Figure 18. *The proper time distribution of simulated $B_s^0 \to D_s^\pm \pi^\mp$ candidates for one year of data at LHCb and two values of ΔM_s. The B_s^0 mesons have been flavour tagged as not oscillated.*

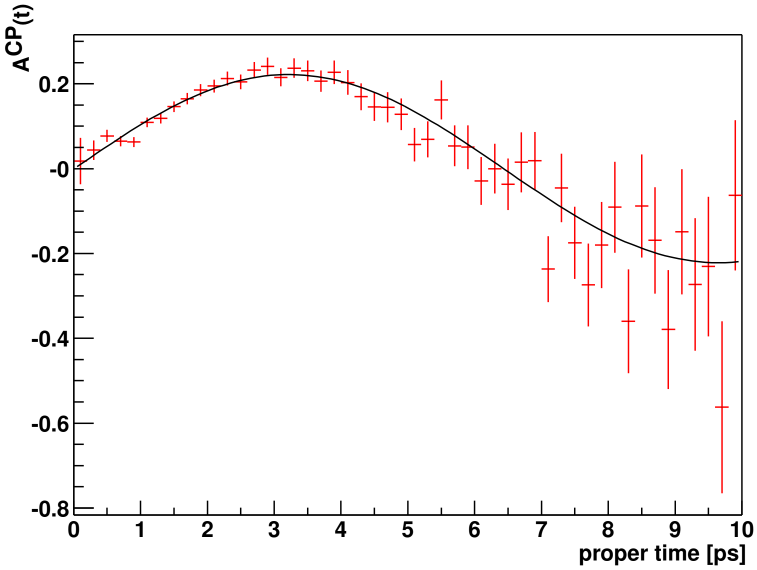

Figure 19. *The CP asymmetry using $B_d^0 \to J/\psi K_S^0$ decays in one year of data at LHCb.*

7.2.3 The B_s^0 Mixing Phase

The B decay channels, $B_s^0 \to J/\psi\phi$ and $B_s^0 \to J/\psi\eta^{(\prime)}$, are the SU(3) analogues of $B_d^0 \to J/\psi K_S^0$. They are both flavour non-specific final states and can be used to determine the B_s^0 mixing phase, the $J/\psi\phi$ being a mixed CP eigenstate and the $J/\psi\eta^{(\prime)}$ a pure CP eigenstate. If only Standard Model processes contribute to B_s^0 oscillations, the CP asymmetry is given by equation (41) with

$$\lambda(B_s^0 \to J/\psi\phi(\eta^{(\prime)})) = \left(\frac{q}{p}\right)_{B_s^0} \left(\frac{\overline{A}}{A}\right)_{J/\psi\phi(\eta^{(\prime)})} \qquad (112)$$

$$= \frac{1-r}{1+r}\left(\frac{V_{tb}^{*}V_{ts}}{V_{tb}V_{ts}^{*}}\right)\left(\frac{V_{cb}V_{cs}^{*}}{V_{cb}^{*}V_{cs}}\right)$$

where r is the ratio of the B_s^0 decay amplitudes into the CP=-1 and CP=+1 states. This leads to

$$\mathrm{Im}\{\lambda(B_s^0 \to J/\psi\phi(\eta^{(\prime)}))\} = \mathrm{Im}\{e^{2i\chi}\} = \sin 2\chi. \tag{113}$$

The Standard Model CKM picture predicts that the B_s^0 mixing phase should be small, $\chi = \eta\lambda^2 \approx -0.04$. Therefore, the observation of a large CP asymmetry in this decay channel would be a striking signal for physics beyond the Standard Model. Similar to the B_d^0 mixing phase, the B_s^0 mixing phase is needed to extract the weak decay phase γ from analyses such as $B_s^0 \to D_s^{\pm}K^{\mp}$ and the combined analysis of $B_d^0 \to \pi^+\pi^-$ and $B_s^0 \to K^+K^-$ decays.

Compared to $B_d^0 \to J/\psi K_S^0$ decays, the $B_s^0 \to J/\psi\phi$ and $B_s^0 \to J/\psi\eta^{(\prime)}$ decay channels present several challenges:

- The mixing frequency ΔM_s of the time-dependent CP asymmetry is very large, requiring excellent proper-time resolution.
- The B_s^0 meson is expected to have a non-negligible decay-width difference, $\Delta\Gamma_s/\Gamma_s$.
- The $B_s^0 \to J/\psi\eta^{(\prime)}$ decay mode, where the η decays predominantly to an all neutral particle final state, requires excellent neutral particle identification and reconstruction.
- Due to the fact that both J/ψ and ϕ are vector mesons, there are three distinct amplitudes contributing to the $B_s^0 \to J/\psi\phi$ decay: two CP even and one CP odd. The two components can be disentangled on a statistical basis by taking into account the distribution of the so-called transversity angle, θ_{tr}, defined in Figure 20.

The results of a study by LHCb using a fit to the transversity angle and B_s^0 mass distribution for $B_s^0 \to J/\psi\phi$ decays indicates that a statistical precision on the B_s^0 mixing phase of $\sigma(\sin\phi_s) \sim 0.06$ and on the decay width difference of $\Delta\Gamma_s/\Gamma_s \sim 0.018$ can be achieved in one year of data taking. A study by ATLAS using the $B_s^0 \to J/\psi\eta^{(\prime)}$ decay mode results in a precision of $\sigma(\phi_s) \sim 0.17$ for one year of data taking at the low luminosity of $10^{33}\mathrm{cm}^{-2}\mathrm{s}^{-1}$ (Ohlsson-Malek 2003).

7.2.4 The Weak Decay Phase

Many methods have been devised to extract the weak decay phase γ and an excellent summary can be found in reference (Fleischer 2002). In general, the methods can be divided into four main categories:

- Method I: time dependent asymmetries,
- Method II: time integrated amplitude relations,
- Method III: isospin symmetry relations, and
- Method IV: Uspin relations.

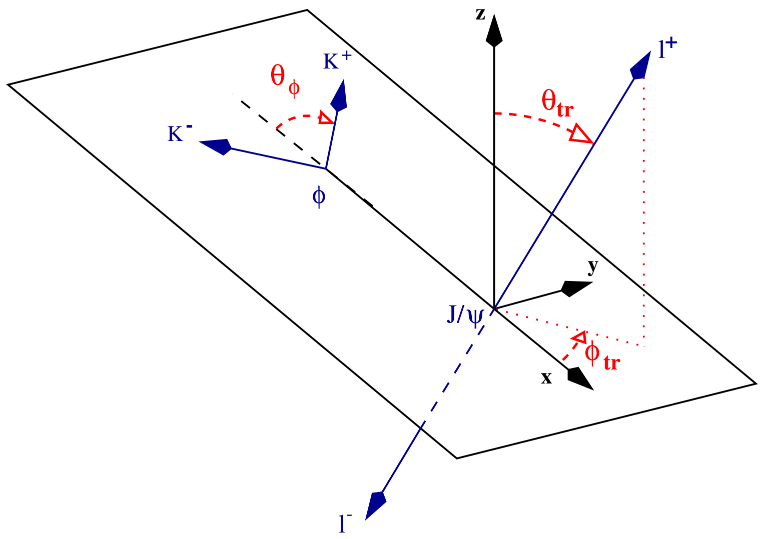

Figure 20. *Definition of the transversity angle used in the LHCb analysis of $B_s^0 \to J/\psi\phi$ decays.*

Methods I and II are mainly model independent as they involve only tree-level decays, whereas III and IV depend on hadronic assumptions and any isospin or Uspin breaking effects. Here, we will illustrate the measurement of the weak decay phase γ in three different ways.

The first way uses the decay mode $B_s^0 \to D_s^\pm K^\mp$, in which the final state is a non-CP eigenstate, and is an example of Method I. The decay can proceed through two tree decay diagrams and their CP conjugated processes, the interference of which gives access to the sum of the weak decay phase and the B_s^0 mixing phase, $\gamma + \phi_s$. In turn, this provides a measurement of γ, if ϕ_s is determined by some other means, for example using $B_s^0 \to J/\psi\phi$ decays. The decay formulae, equations (20) and (21), can be applied with $|\lambda| = |\overline{\lambda}| \approx 0.5$ and $arg\{\lambda\} = \Delta + (\gamma + \phi_s)$ and $arg\{\overline{\lambda}\} = \Delta - (\gamma + \phi_s)$ where Δ denotes the strong phase difference between the two tree diagrams. Experimentally, a potentially large background arises due to the $B_s^0 \to D_s^\pm \pi^\mp$ decay mode which has more than 10 times the branching fraction of $B_s^0 \to D_s^\pm K^\mp$. The LHCb RICH detectors, therefore, provide a powerful means to separate out the $B_s^0 \to D_s^\pm \pi^\mp$ and $B_s^0 \to D_s^\pm K^\mp$ contributions as illustrated in Figure 21. In the LHCb study, a simultaneous fit is performed to the $B_s^0 \to D_s^\pm \pi^\mp$ and $B_s^0 \to D_s^\pm K^\mp$ decays to determine the parameters ΔM_s, $|\lambda| = |\overline{\lambda}|$, $arg\{\lambda\}$, $arg\{\overline{\lambda}\}$ and the mistag fraction. ΔM_s and the mistag fraction are effectively determined from the flavour asymmetry in the $B_s^0 \to D_s^\pm \pi^\mp$ event sample, while being applied at the same time to measure the CP asymmetry in the $B_s^0 \to D_s^\pm K^\mp$ sample. An example of the $B_s^0 \to D_s^\pm K^\mp$ asymmetries obtained after 5 years of data taking are shown in Figure 22. The value of the weak phase $\gamma + \phi_s$ is extracted from the difference of the fitted parameters $arg\{\lambda\} - arg\{\overline{\lambda}\}$. The expected statistical uncertainty on $\gamma + \phi_s$ for one year of data is $\sigma(\gamma + \phi_s) \sim$ 14-15 degrees for values of $\gamma + \phi_s$ ranging between 55 and 105 degrees.

Our second illustration to extract γ is an example of Method II and relies on the measurement of three time-integrated decay rates, $B_d^0 \to \overline{D^0}(K^+\pi^-)K^{0*}$, $B_d^0 \to D^0_{\rm CP}(K^+K^-)K^{0*}$, $B_d^0 \to D^0(\pi^+K^-)K^{0*}$, and their CP conjugates. $D^0_{\rm CP} = (D^0 + \overline{D^0})/\sqrt{2}$ denotes the CP even eigenstate of the D^0-$\overline{D^0}$ system and $K^{0*} \to K^+\pi^-$. The method is theoretically clean as the decays involve tree-level diagrams, which interfere due to the presence of

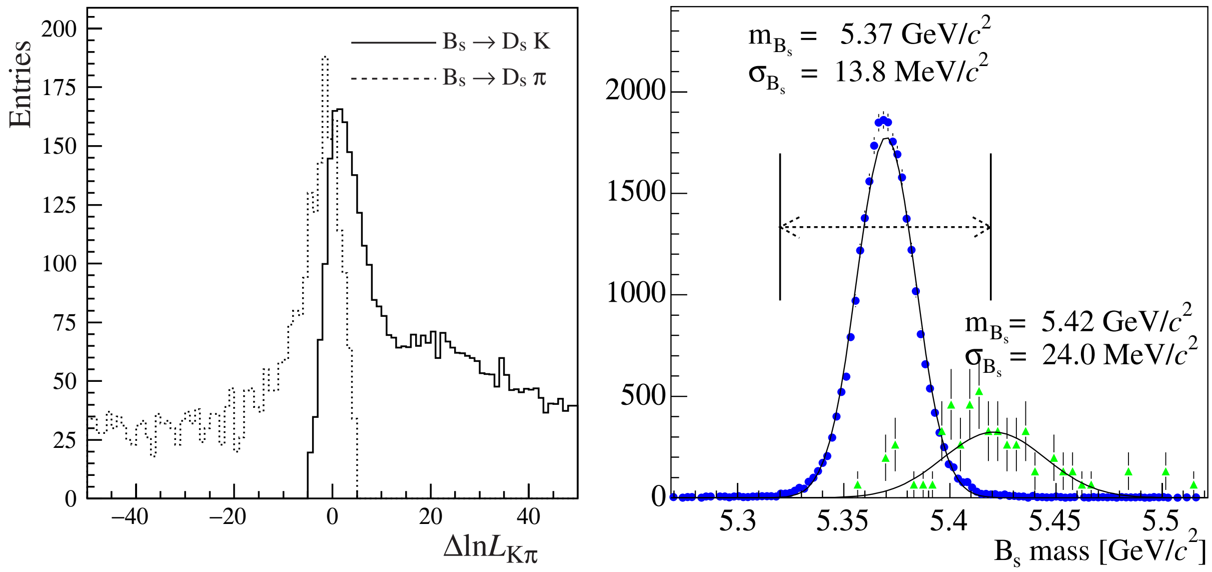

Figure 21. *The difference in log-likelihood between the RICH hypotheses for the K and π coming directly from the B_s^0 in $B_s^0 \to D_s^{\pm} K^{\mp}$ and $B_s^0 \to D_s^{\pm}\pi^{\mp}$ decays (left) and the B_s^0 mass distribution for selected $B_s^0 \to D_s^{\pm} K^{\mp}$ candidates (right). Also shown (right) are the misidentified $B_s^0 \to D_s^{\pm}\pi^{\mp}$ events normalised to the visible branching ratios.*

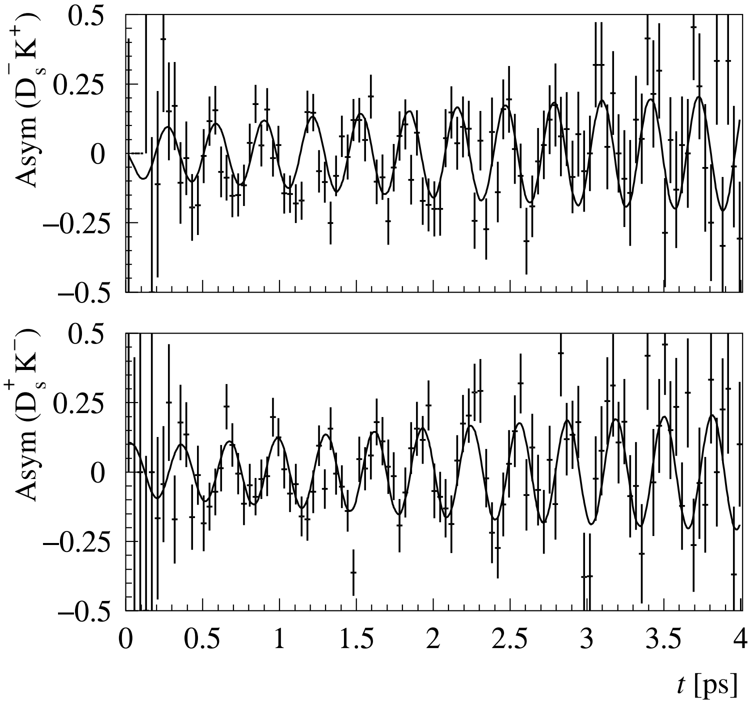

Figure 22. *Time dependent B_s^0-$\overline{B_s^0}$ asymmetry of $D_s^- K^+$ (top) and $D_s^+ K^-$ (bottom) events for $\Delta M_s = 20\,\mathrm{ps}^{-1}$ and 5 years of data.*

$D^0 - \overline{D^0}$ mixing. The value of γ extracted through this method is therefore sensitive to any new physics in $D^0 - \overline{D^0}$ oscillations. The relations between the six decay rates are used to extract the weak decay phase γ as well as the strong phase difference between $B_d^0 \to D^0 K^{0*}$ and $B_d^0 \to \overline{D^0} K^{0*}$ decays. An advantage of this analysis is that no proper time information or tagging is required. However, the visible branching ratios are low, for example $\mathrm{Br}(B_d^0 \to D_{\mathrm{CP}}^0(K^+K^-)K^{0*}) \sim 0.2 \times 10^{-6}$, resulting in $\sim$ 0.6k events reconstructed per year. The expected statistical precision on γ after one year of data taking is $\sigma(\gamma)$ =9-7 degrees for values of γ in the range 55 to 105 degrees. The sensitivity is independent on the value of the strong phase difference, but decreases by approximately 1 degree for a change in background level of 20%.

Our final illustration is an example of Method IV which uses Uspin symmetry (replacement of all d quarks with s quarks) to relate B_d^0 and B_s^0 decays. The decay modes we shall consider are $B_d^0 \to \pi^+\pi^-$ and $B_s^0 \to K^+K^-$. Under the assumption that the strong interaction dynamics remains invariant under this interchange, the relative contributions of the penguin process with respect to the tree process are identical in the two decay modes and γ can be determined from the time-dependent CP asymmetry for B_d^0 and $\overline{B_d^0}$ decaying into $\pi^+\pi^-$ and that for B_s^0 and $\overline{B_s^0}$ decaying into K^+K^-. Therefore, the value of γ extracted from this method is sensitive to any new physics in the penguin diagrams. Uspin symmetry can be also tested by using the values of ϕ_d and ϕ_s obtained from the CP asymmetries measured with $B_d^0 \to J/\psi K_S^0$ and $B_s^0 \to J/\psi\phi$ decays. Experimentally, a crucial requirement for the analysis of $B_d^0 \to \pi^+\pi^-$ and $B_s^0 \to K^+K^-$ decays is the ability to suppress other B hadron decays with the same two track topology and which may exhibit their own CP asymmetries. In LHCb, the rejection of these backgrounds relies on the performance of the RICH particle identification and on the invariant mass resolution. An example of the invariant mass distribution for selected and triggered $B_s^0 \to K^+K^-$ decays obtained by LHCb is shown in Figure 23. In order to extract the weak decay phase γ, a fit is performed to the $B_d^0 \to \pi^+\pi^-$ and $B_s^0 \to K^+K^-$ CP asymmetries to measure the four observables $\mathcal{A}_{\mathrm{CP}}^{dir}(B_d^0 \to \pi^+\pi^-)$, $\mathcal{A}_{\mathrm{CP}}^{mix}(B_d^0 \to \pi^+\pi^-)$, $\mathcal{A}_{\mathrm{CP}}^{dir}(B_s^0 \to K^+K^-)$ and $\mathcal{A}_{\mathrm{CP}}^{mix}(B_s^0 \to K^+K^-)$. These four observables depend on the B_d^0 mixing phase ϕ_d, the B_s^0 mixing phase ϕ_s, the weak decay phase γ and the amplitudes and phases of the penguin to tree ratios. In the limit of exact Uspin symmetry of the strong interaction, the amplitude (d) and phase (θ) of the penguin to tree ratio in $B_d^0 \to \pi^+\pi^-$ and the equivalent quantities in $B_s^0 \to K^+K^-$ decays are the same. In this case, the measurements of the four CP asymmetry observables provide a determination of γ, if ϕ_d and ϕ_s are taken from elsewhere. The expected sensitivity on γ for one year of data is $\sigma(\gamma) \sim 5$ degrees assuming the Standard Model values of $\Delta\Gamma_s/\Gamma_s = 0.1$ and $\Delta M_s = 20\,\mathrm{ps}^{-1}$, and $d = 0.3$ and $\theta = 160$ degrees. An example of the confidence regions in the (d, γ) plane for one year of data, together with the one-dimensional experimental probability density functions is shown in Figure 24.

7.3 Tests for New Physics

There are many ways of looking for new physics outside of the Standard Model description of the CKM matrix (Stone 2001). A generic approach is to look for inconsistencies between the different kinds of measurements used to determine the apex of the unitarity triangle. For example, new physics outside the Standard Model could reveal itself as discrepancies among the values of ρ and η derived from independent determinations using the magnitude measurements ($|V_{ub}/V_{cb}|$ and $|V_{td}/V_{ts}|$), or from the different CP violation measurements in B_d^0, B_s^0 and K_L^0 decays. Another interesting generic approach is to express the CKM matrix in terms of four phases instead of the Wolfenstein parameters and to perform

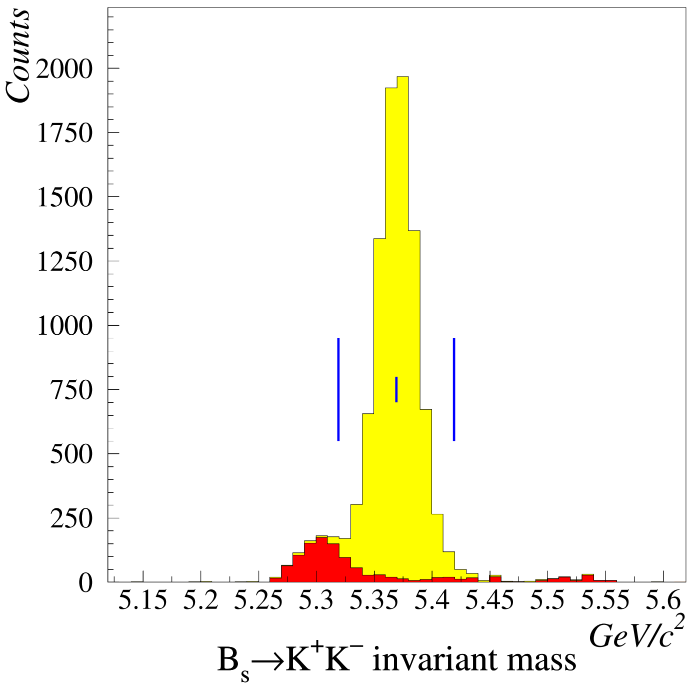

Figure 23. *Invariant mass distribution for selected $B_s^0 \to K^+K^-$ candidates. The light-shaded (yellow) region is the signal and the dark (red) one represents background from B decays with the same two charged track topology.*

checks between them. Silva and Wolfenstein have shown that the relationship

$$\sin\chi = \frac{\lambda^2 \sin\beta \sin\gamma}{\sin(\beta+\gamma)} \tag{114}$$

is a critical check of the Standard Model. The final approach is to compare CP phases extracted from different exclusive B decay channels. For example, a recently observed difference by the Belle collaboration between the B_d^0 mixing phase obtained using $B_d^0 \to J/\psi K_S^0$ decays (tree diagram) and that from $B_d^0 \to \phi K_S^0$ decays (pure penguin diagram) may be an indication that new physics is just around the corner (Belle 2003).

At the LHC, the B_s^0 meson plays an essential rôle to disentangle new physics from that of the Standard Model. Let us consider the three ways we have discussed in these lectures to extract the weak decay phase γ. The value of γ measured using $B_s^0 \to D_s^{\pm}K^{\mp}$ decays will not be affected by the possible existence of new particles. However, the combined analysis of $B_d^0 \to \pi^+\pi^-$ and $B_s^0 \to K^+K^-$ decays makes explicit use of the penguin processes where new particles can contribute to the loops. Equally, new physics in D^0-$\overline{D^0}$ mixing could affect the value of γ extracted from the analysis of $B_d^0 \to D^0K^{0*}$ decays. From these three measurements, it will be possible to determine γ and, together with the measurement of $|V_{ub}|$, extract the CKM parameters A, ρ and η even in the presence of new physics. In addition, it will be possible to extract the contribution of new physics to the oscillations and penguins. A possible scenario after one year of data taking at LHCb is shown in Figure 25. The measured value of γ could disagree with that obtained from the current Standard Model analysis of the CKM parameters using processes generated

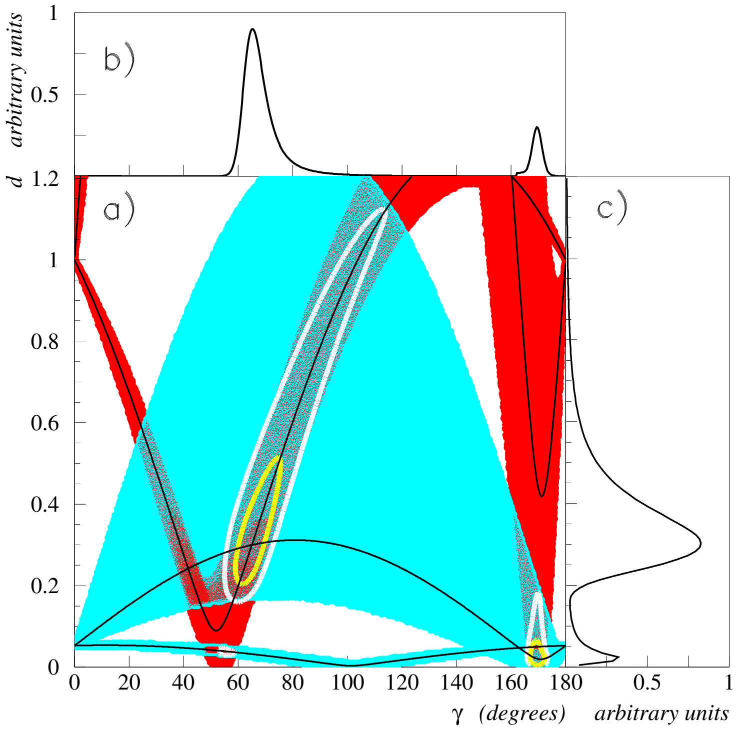

Figure 24. *a) Confidence regions in the (d, γ) plane; the darker (red) bands indicate the region obtained from $B_d^0 \to \pi^+\pi^-$; the lighter (cyan) bands indicate the region obtained from $B_s^0 \to K^+K^-$ and the black solid curves represent the exact analytical calculations. The deformed ellipses enclose the 68% and 95% confidence regions obtained by using all constraints. b) and c) are the probability density functions for γ and d respectively.*

by tree and box diagrams. This would be a clear signal for the existence of new physics in the B^0-$\overline{B^0}$ oscillations and would allow the separation of the new physics from that of the Standard Model.

7.4 Rare B Decays

Very rare B decays are an excellent place to search for new physics (Abbaneo 2003) (Nir 1999). Figure 2c) shows the basic Standard Model diagram for these processes which, in general, tend to have small branching ratios, for example $\mathrm{Br}(B_d^0 \to K^*\gamma) \sim 4 \times 10^{-5}$, $\mathrm{Br}(B_d^0 \to K^{0*}\mu^+\mu^-) \sim 10^{-6}$ and $\mathrm{Br}(B_d^0 \to \mu^+\mu^-) \sim 10^{-10}$. However, in the presence of new physics, new fermion-like particles can replace the quarks or new gauge-like particles can replace the W, thereby increasing the branching fractions significantly. The exclusive processes are also sensitive to new physics in observables other than the branching fractions, such as photon polarization, forward-backward asymmetries and CP asymmetries. Their branching fractions also depend on the CKM matrix elements $|V_{ts}|$ and $|V_{td}|$, thereby providing another consistency check of the unitarity of the CKM matrix. The main impact in the LHC era on the study of rare decays will be to observe rare B_s^0 decays and to provide a radical increase in statistics. $B \to \mu^+\mu^-$ decays will only be observed before the LHC era if it is enhanced drastically by the presence of new physics. The study of rare B decays in the LHC era is at a preliminary stage, mainly

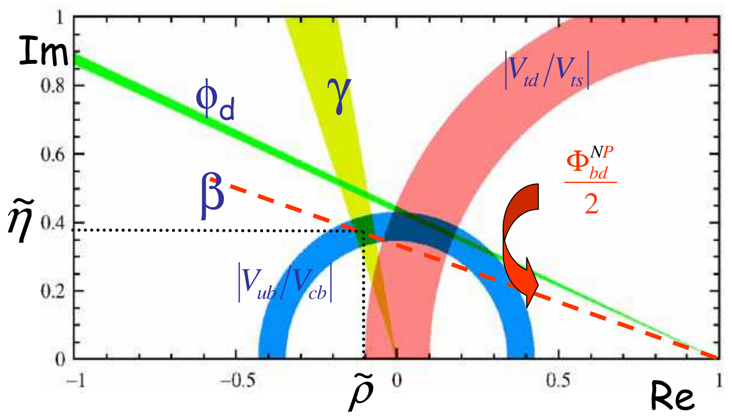

Figure 25. *A possible scenario for the allowed region in the $\tilde{\rho}$-$\tilde{\eta}$ plane after one year of data taking at LHCb. The contribution from new physics to the B^0-$\overline{B^0}$ oscillation is indicated.*

due to estimating the size of the background when the branching ratios are so small. However, it is expected that all the next generation experiments will have significant statistics for decay channels that have two leptons in the final state, such as $B \to \mu^+\mu^-$, $B_d^0 \to K^{0*}\mu^+\mu^-$ and $B_s^0 \to \phi\mu^+\mu^-$ and for the radiative rare B decays, such as $B_d^0 \to K^*\gamma$ and $B_s^0 \to \phi\gamma$ (Ahmadov 2000).

8 Conclusions

An exciting time for B physics has just commenced. The first experimental phase has recently provided the first observation of CP violation in the B system by BaBar and Belle. These experiments, together with CDF and D0 at the Tevatron collider, will measure the CKM parameters with unprecedented precision. The next generation of B experiments (LHCb, BTeV and the general purpose experiments, ATLAS and CMS) will start to become operational in 2007 and will be the ultimate source for B physics studies. Their goal is to thoroughly test the internal consistency of the Standard Model, to search for the necessary new physics beyond and to disentangle the new physics from the Standard Model physics. I certainly look forward to the next 10-15 years of B physics results and hope that new physics will reveal itself first in the virtual world of the B sector.

Acknowledgments

I thank the organizers of the school for inviting me to give these lectures and for their hospitality. T.Nakada and R.Thorne are deeply acknowledged for many useful comments.

References

Abbaneo, D. et al (2003), *The CKM Matrix and the Unitarity Triangle*, editors M.Battaglia et al, hep-ph/0304132v1.

Ahmadov, A. et al (2000), *Proceedings of the Workshop on Standard Model Physics (and more) at the LHC*, CERN 2000-04.

Amato, S. (1998), *LHCb Technical Proposal*, CERN/LHCC/98-4.

Antunes Nobrega, R. (2003), *LHCb Reoptimized Detector Design and Performance*, CERN/LHCC/2003-030.

BaBar Collaboration [Aubert, B. et al] (1998), *The BaBar Physics book*, editors P.F.Harrison and H.R.Quinn, SLAC-R-504.

BaBar Collaboration [Aubert, B. et al] (2001), *Phys. Rev. Lett.* **87**, 091801.

BaBar Collaboration [Aubert, B. et al] (2002), *Phys. Rev. Lett.* **88**, 221803.

Belle Collaboration [Abe, K. et al] (2001), *Phys. Rev. Lett.* **87**, 091802.

Belle Collaboration [Abe, K. et al] (2003), *submitted to Phys. Rev. Lett.*, hep-ex/0308035.

Browder, T. (2003), *Proceedings of the XXI International Symposium on Lepton and Photon Interactions at High Energies*, Fermilab August 2003.

Cabibbo, N. (1963), *Phys. Rev. Lett.* **10**, 531.

Charles, J. et al [CKMFitter] (2003), http://ckmfitter.in2p3.fr/.

Christenson, J.H. et al (1964), *Phys. Rev. Lett.* **13**, 138.

Drobychev, G.Y. (2002), *Update to Proposal for an Experiment to Measure Mixing, CP Violation and Rare Decays in Charm and Beauty Particle Decays at the Fermilab Collider - BTeV*, BTeV-doc-316-v3.

Fleischer, R. (2002), *Physics Reports* **370**, 537.

Harr, R. (2003), *Proceedings of Beauty 2003, 9th International Conference on B Physics at Hadron Machines*, Pittsburgh October 2003.

HFAG [Heavy Flavour Averaging Group] (2003), http://qqq.slac.stanford.edu/xorg/hfag/.

Jarlskog, C. (1986), *Proceedings of the 1986 Recontre de Moriond on "Progress in Electroweak Interactions"* editor J.Tran Thanh Van 389.

Kobayashi, M. and Maskawa, K. (1972), *Prog. Theor. Phys.* **49**, 282.

Nakada, T. (2002), *Surveys in High Energy Physics* **17**, 3.

Nir, Y. (1999), *XXVII SLAC Summer Institute on Particle Physics*, hep-ph/9911321.

Nir, Y. (2001), *55th SUSSP on Heavy Flavour Physics.*

Ohlsson-Malek, F. (2003), *Proceedings of Flavour Physics and CP Violation Conference* Paris June 2003.

Particle Data Group [Hagiwara, K. et al] (2002), *Phys. Rev. D* **66**, 1.

Particle Data Group [Hagiwara, K. et al] (2003), http://pdg.lbl.gov/.

Paulini, M. (2003), *Proceedings of the Physics at the LHC Conference* Prague July 2003.

Sakharov, A.D. (1967), *JETP Lett.* **5**, 24.

Salam, G.P. (2002), *Proceedings of the X International Workshop on Deep Inelastic Scattering* Cracow Poland July 2002, hep-ph/0207147.

Schubert, K. (2003), *Proceedings of the XXI International Symposium on Lepton and Photon Interactions at High Energies*, Fermilab August 2003.

Shaposhnikov, M.E. (1986), *JETP Lett.* **44**, 364.

Stone, S. (2001), hep-ph/0111313 and references therein.

Virdee, T. (2003), *this volume.*

Wolfenstein, L. (1964), *Phys. Rev. Lett.* **13**, 562.

Wolfenstein, L. (1983), *Phys. Rev. Lett.* **51**, 1945.